

An archival search for white dwarf pulsars

by

Margaret Ridder

A thesis submitted in partial fulfillment of the requirements for the degree of

Master of Science

Department of Physics

University of Alberta

© Margaret Ridder, 2021

Abstract

AR Sco is the first known white dwarf pulsar and currently there is no definitive model for its emission or evolution. This type of binary system could be a critical step in the formation of magnetic cataclysmic variables, a type of accreting white dwarf/M dwarf binary system. In this thesis, I outline a new method of finding AR Sco twins. Since AR Sco was originally classified as a δ Scuti pulsating variable star, I examine catalogs of these stars from optical surveys. In these catalogs, I find possible candidates that are more blue in color and are dim compared to the rest of the sample since these qualities mimic those of AR Sco. We apply these selection criteria to catalogs from the All-sky Automated Survey for Supernovae, the Zwicky Transient Facility, and Rodríguez et al. (2000). In addition, I analyze *Gaia* data using a similar method, but this was limited by the relative lack of time-series data. I also try to identify X-ray and radio counterparts to our possible candidates. Modeling the distribution of δ Scutis in the Galaxy, I find that our catalogs are the most complete for high-amplitude variables. Using the high-amplitude subset of our possible candidates, I calculate an upper and lower limit on the number of δ Scutis in the Galaxy that could be misidentified AR Sco twins. In the future, I will ask for follow-up time on *Chandra* X-ray Observatory, Very Large Array, and Gemini to study possible candidate twins.

Preface

This thesis is an original work by Margaret Ridder under the supervision of Craig Heinke. In Section 4.1, where the space density of stars is calculated, I had the generous help of F. Fontinele Nunes and L. Olifer in the analytical integration and change in coordinate systems. Finally, the radio flux of QS Vir (Section 2.5.1) was calculated by A. Hughes and G. Sivakoff.

Most days I find out why I was wrong instead of why I was right.

– Craig O. Heinke, 2021.

One man's trash is another man's treasure.

– Unknown.

Acknowledgements

This research has made use of data and/or software provided by the High Energy Astrophysics Science Archive Research Center (HEASARC), which is a service of the Astrophysics Science Division at NASA/GSFC. I acknowledge the use of public data from the *Swift* data archive and data supplied by the UK Swift Science Data Centre at the University of Leicester. This work has made use of data from the European Space Agency (ESA) mission *Gaia* (<https://www.cosmos.esa.int/gaia>), processed by the *Gaia* Data Processing and Analysis Consortium (DPAC, <https://www.cosmos.esa.int/web/gaia/dpac/consortium>). Funding for the DPAC has been provided by national institutions, in particular the institutions participating in the *Gaia* Multilateral Agreement. This work is partly based on observations obtained with the Samuel Oschin 48-inch Telescope at the Palomar Observatory as part of the Zwicky Transient Facility project. ZTF is supported by the National Science Foundation under Grant No. AST-1440341 and a collaboration including Caltech, IPAC, the Weizmann Institute for Science, the Oskar Klein Center at Stockholm University, the University of Maryland, the University of Washington, Deutsches Elektronen-Synchrotron and Humboldt University, Los Alamos National Laboratories, the TANGO Consortium of Taiwan, the University of Wisconsin at Milwaukee, and Lawrence Berkeley National Laboratories. Operations are conducted by COO, IPAC, and UW. This research has made use of the CIRADA cutout service at URL.cutouts.cirada.ca, operated by the Canadian Initiative for Radio Astronomy Data Analysis (CIRADA). CIRADA is funded by a grant from the Canada Foundation for Innovation 2017 Innovation Fund (Project 35999), as well as by the Provinces of Ontario, British Columbia, Alberta, Manitoba and Quebec, in collaboration with the National Research

Council of Canada, the US National Radio Astronomy Observatory (NRAO) and Australia's Commonwealth Scientific and Industrial Research Organisation. This work also makes use of data taken with the Karl G. Jansky Very Large Array, run by the NRAO. The NRAO is a facility of the National Science Foundation operated under cooperative agreement by Associated Universities, Inc. This work as well made use of data from the All-sky Automated Survey for Supernovae (ASAS-SN), run by Ohio State University. I would also like to acknowledge the use of TOPCAT (Taylor, 2005) as it came in handy for every part of the analysis in this thesis.

Table of Contents

1	Introduction	1
1.1	δ Scuti variable stars	1
1.2	White dwarfs	2
1.3	Cataclysmic variables	4
1.3.1	Weakly magnetic	4
1.3.2	Strongly magnetic	6
1.4	AR Sco: the first white dwarf pulsar	7
1.5	The origin of bright radio sources in our galaxy	9
2	Analyzing δ Scutis from ASAS-SN	11
2.1	The dataset	11
2.2	Candidate selection with luminosity and color	12
2.2.1	δ Scuti Period Luminosity Relation	12
2.2.2	Gaia color magnitude diagram	14
2.3	Power spectra	16
2.4	Looking for radio and X-ray counterparts	16
2.5	Discussion	20
2.5.1	CVs in ASAS-SN	22
2.6	The importance of accurate distances	22
3	Other searches for candidates	24
3.1	Rodríguez et al. (2000) Catalog	24
3.2	The Zwicky Transient Facility	26
3.3	Gaia	32
3.3.1	Candidate selection by amplitude	36
4	Population estimate of AR Scos in the Milky Way	39
4.1	The space density of δ Scutis	39
4.2	Completeness of different amplitudes	42
4.3	Population lower limit	43
4.4	Population upper limit using ASAS-SN, ZTF, and Rodríguez et al. (2000)	45
4.5	Comparison to quiescent BHXB population	46
5	Conclusion	47
	References	50

List of Tables

2.1	2MASS photometric flags	12
2.2	Possible ASAS-SN candidates.	21
3.1	Unlikely, but possible Rodríguez et al. (2000) candidates . . .	26
3.2	Possible ZTF candidates	31
3.3	X-ray sources in the Gaia sample	36
3.4	X-ray luminosities for CVs in Gaia EDR3	36
3.5	Preliminary Gaia candidates	37
3.6	High-amplitude δ Scutis in Gaia	38

List of Figures

1.1	AR Sco's spectral energy distribution	8
1.2	$L_X - L_R$ plane	10
2.1	ASAS-SN PLR	14
2.2	ASAS-SN CMD, Gaia color	15
2.3	Example of a poor power spectrum	17
2.4	Example of a less noisy power spectrum	18
2.5	ASAS-SN X-ray luminosity limit	19
2.6	ASAS-SN radio luminosity limit	20
3.1	Coordinate error in Rodríguez et al. (2000)	25
3.2	Rodríguez et al. (2000) PLR	26
3.3	Rodríguez et al. (2000) CMD	27
3.4	ZTF PLR	29
3.5	ZTF CMD	30
3.6	ZTF X-ray luminosity limit	32
3.7	ZTF radio luminosity limit	33
3.8	X-ray light curve of Swift source, Target ID: 49932	34
3.9	Gaia sources in HEASARC search	35
4.1	Population density fit to Rodríguez et al. (2000)	41
4.2	Population model compared to ASAS-SN	42
4.3	The fit to only the high-amplitude δ Scutis from Rodríguez et al. (2000).	43
4.4	The fit from Figure 4.3 to high-amplitude ASAS-SN δ Scutis.	44
4.5	The fit from Figure 4.3 to high-amplitude ZTF δ Scutis.	45

Chapter 1

Introduction

Here I cover the basics required for understanding white dwarf pulsars and the search I conduct in the next chapters. I begin with δ Scutis, a common variable star that I will examine many of them in my search. On the subject of white dwarf pulsars themselves, I start with white dwarfs, introduce cataclysmic variables (binaries including a white dwarf), and lastly describe the first white dwarf pulsar discovered, AR Sco. Finally, I discuss odd radio sources in the galaxy and their relation to AR Sco.

1.1 δ Scuti variable stars

Pulsating variables are interesting on their own, but here I will only provide a brief introduction into δ Scutis and how they pulsate. Variable stars are not the root subject of this thesis, but the data in later chapters come from δ Scuti catalogs.

δ Scutis are fairly common pulsating variable stars of spectral type A - F. On the Hertzsprung-Russell (HR) diagram (a plot of color vs luminosity), δ Scutis are just below the RR Lyrae instability strip. δ Scutis are near temperatures of 8000 K and 10 times L_{\odot} (Carroll & Ostlie, 2007). As an example of their population size, roughly 8000 δ Scutis in our dataset were discovered in Gaia DR2 (Rimoldini et al., 2019). They tend to be short-period and low-amplitude (Rodríguez et al., 2000; Hansen et al., 2004). If we look at trends in the catalog from the Zwicky Transient Facility (ZTF), the majority have periods of at most 0.2 days, but cluster between 0.05 and 0.1 days. The peak

in the amplitude distribution is below 0.1 mag, but it is not uncommon to see amplitudes up to 1 mag. The pulsations are due to the partial ionization of He outside the core of these stars. Ionization prevents the gas in this region of the star from reaching hydrostatic equilibrium and the instability is manifested by stellar pulsation. In an ionizing mass element, the temperature rises upon compression. The opacity in turn increases and prevents further flow of radiation outward, making hydrostatic equilibrium impossible (Hansen et al., 2004). In more technical terms, the pulsation in δ Scutis is self-excited by the so-called κ mechanism (Bowman, 2017).

1.2 White dwarfs

In this section, we'll direct our attention more towards the main topic of this work by discussing white dwarfs. To produce a white dwarf (WD), we have to begin with a star $\leq 8M_{\odot}$ (Bradt, 2008; Carroll & Ostlie, 2007). Over the course of a low mass star's life it will fuse consecutively heavier and heavier elements, but it will stop short of iron, unlike high mass stars. If the star has a helium (He) core mass greater than $0.5M_{\odot}$ (Carroll & Ostlie, 2007), it will generate carbon and oxygen, the end of fusion. We refer to a core like this as "inert." Above the core are first, a shell of He fusion, inert He, a shell of hydrogen (H) fusion, and finally inert H. The high temperature in these shells expands the outer layers of the star. Consequently, they are less gravitationally bound to the star itself and are easily released into space (Hansen et al., 2004; Carroll & Ostlie, 2007). The leftover core is the WD. Smaller initial He cores will actually never activate fusion and at the end the star's life, it will produce a He WD instead (Carroll & Ostlie, 2007).

Normally, stars are in a balance between gravity and the outward pressure of fusion. Inside, the pressure is linearly dependent on temperature (explained by the ideal gas law; Hansen et al., 2004). Since WDs are not fusing elements in their core, the only thing preventing them from collapsing is electron degeneracy pressure. Electrons, being fermions, cannot occupy the same position in phase space. The associated pressure with this phenomenon for

non-relativistic electrons, like those in a WD, goes as $P \propto \rho^{5/3}$ (Bradt, 2008). This is the rough equation of state for the interior of a WD. Unlike the ideal gas law, this equation of state (EOS) is independent of temperature, because of degeneracy. White dwarfs collapse when they reach ≈ 1.4 solar masses, known as the Chandrasekhar mass limit (Bradt, 2008; Carroll & Ostlie, 2007).

The strong gravitational pull of a WD stratifies the interior; heavier elements sink to the center while lighter elements float to the top, meaning that any H or He that is left behind on the core will float on the surface of a WD. This is the reason behind why there are prominent H absorption lines in most WD spectra (Carroll & Ostlie, 2007), which are significantly broader than those seen in main sequence stars. This is due primarily to pressure broadening (Dimitrijević et al., 2011; Hellier, 2001). WD atmospheres are subject to intense pressures. When the atoms in their atmospheres are packed so tightly together, the number of interactions with neighboring atoms increases, resulting in an uncertainty in their electron's energy states (Hellier, 2001). Consequently, each absorption line widens.

While WDs are not the most extreme compact object we know of, they still possess strong magnetic fields, the full range being 10^3 G (tentatively) to 10^9 G (Ferrario et al., 2015). The field tends to be dipolar (Hansen et al., 2004), but as they get stronger, they can become multipolar (Ferrario et al., 2015). Around 2% of highly magnetic WDs (those more than 10^6 G) reside in a binary system with a main-sequence (MS) companion, while up to a quarter of cataclysmic variables (described in the next section) house one (Ferrario et al., 2015). Magnetic field generation in WDs is still an area of active research. However, there are a few leading ideas. It is possible that in the common envelope phase of binary evolution (where the two stars share a diffuse outer layer), differential rotation inside the envelope generates a magnetic field by way of the dynamo mechanism (Ferrario et al., 2015). The fossil field hypothesis cannot, however, be ignored: the magnetic field from earlier stages of stellar evolution could be left behind inside the WD (Ferrario et al., 2015; Wickramasinghe & Ferrario, 2005).

1.3 Cataclysmic variables

Isolated WDs slowly cool over the course of billions of years (Hansen et al., 2004). However, in a binary they may accrete matter from their companion, which is the case for cataclysmic variables (CVs). In a CV, a WD is paired with a MS star of M or K spectral type. CVs are a later stage of binary evolution. At the formation of the binary, one of these stars must be more massive than the other in order for it to evolve faster. Once this star expands as it evolves, its matter will spill over onto the lower mass star so fast that it overfills its Roche lobe, a figure-8 region around the binary that marks equal gravitational potential. This rapid overflow creates a diffuse common envelope surrounding both stars. Through friction, the envelope shrinks the orbital distance closer together until the orbital period is on the order of a few hours. The envelope is then gradually expelled leaving a detached WD/red dwarf binary that may later become a CV (Hellier, 2001).

To begin mass transfer in a CV, the companion must expand to fill its Roche lobe, at which point matter flows through the first Lagrange point (where the equipotential lines cross; Hellier, 2001). The manner of accretion onto the WD is determined by the strength of the WD’s magnetic field. In weakly magnetic systems, matter from the donor flows into an accretion disc around the WD. Then, in a process I will discuss in the following subsection, the WD is fed by infalling matter from the disc. For highly magnetic systems, matter from the donor cannot form a disc and instead flows along the field lines to the magnetic poles of the WD.

1.3.1 Weakly magnetic

The spectrum of weakly magnetic systems is dominated by blackbody radiation originating from the accretion disc. Broad H lines are visible, indicating the speed of the matter within the disc. An important feature of CVs with a disc is the “bright spot.” As material from the donor star meets the disc, it creates a luminous shock (Robinson, 1976) that is responsible for around 30% of the light emanating from the system (Hellier, 2001). This is evident in

the light curves of eclipsing CVs, in which there is a hump in the curve where the bright spot is eclipsed. The bright spot is also responsible for the rapid, non-periodic flickering characteristic of CVs.

There are various types of CVs that all undergo outbursts, which are significant (and sometimes recurring) brightening events in their light curves. To be clear, there are different mechanisms behind the first and the rest of these outbursts, but they have confusingly been given similar names. Here, we will discuss novae, recurrent novae, and dwarf novae. A nova outburst is a product of momentary ignition of fusion on the surface of the WD (Hellier, 2001; Zorotovic & Schreiber, 2020). By accreting material from the donor, the WD grows its H atmosphere until the boundary between the atmosphere and core ignites, rapidly fusing H into He. This is possible because the WD EOS permits temperature increases without an increase in pressure. However, there is a maximum temperature before the gas quickly expands and ejects the H shell. The increase in brightness ($M_V \lesssim -7$ mag) is what we call the nova and should happen eventually for any kind of CV (Warner, 2003). Dwarf novae by contrast are much less dramatic. The increase in brightness is simply due to an increase in the accretion rate that heats the disc and the WD surface. The timescales and magnitudes of each type vary widely. Regular novae occur every 10,000 to 100,000 years. Recurrent novae, on the other hand, happen on the scale of decades to centuries with an amplitude of 7 - 14 magnitudes. The lowest amplitude type of outburst is the dwarf nova. It is also the most frequent, occurring every 10s of days to 10s years (e.g. WZ Sge, Patterson et al. (2002)), and the system will brighten by 2 - 6 magnitudes (Wargau, 1985). The outbursts are not necessarily periodic and the duration of each one can vary (Hellier, 2001).

A momentary increase in the accretion rate onto the WD can result in a dwarf nova. Here, I will endeavor to provide a brief, qualitative summary of the disc instability model (DIM), the source of this increased accretion rate. Accretion discs in CVs are unstable and have two distinct states (Lasota, 2001; Dubus et al., 2018). Thermal instability is the term used to describe the disc's tendency to flip between a cold, low-viscosity state and a hot, high-viscosity

state. Ionized (hot) material tends to move along magnetic field lines, but in a disc, these lines can become stretched out and magnified due to the different orbital speeds of material closer and farther from the WD. This disrupts the orderly flow of material and is referred to as magnetic turbulence. Magnetic turbulence mimics the kind of viscosity stemming from atomic interactions, which ionized material lacks. If the density of the disc increases with added material from the donor star, then temperature will increase accordingly. At a certain point the gas will ionize and the addition of magnetic turbulence increases the viscosity. The effect of viscosity is to spread out the disc through the transfer of angular momentum: the inner parts draw nearer to the WD, and the outer parts move farther away. After the additional material is dumped onto the WD the density of the disc decreases and the disc cools, bringing it back to a temperature where H can recombine (Hellier, 2001). During an outburst then, the disc is hot, ionized, and hence, viscous. During quiescence, the disc is cold and unionized.

1.3.2 Strongly magnetic

As mentioned above, matter flows along magnetic field lines in CVs with a highly magnetized WD. Moderately magnetic WDs may still have an accretion disc, but at some distance to the WD surface, the material from the disc will be dragged along the magnetic field lines before being accreted. These are known as intermediate polars (IPs). For highly magnetic WDs, no accretion disc is possible and all of the material flows down onto the poles. These systems are called polars. As mentioned in the previous section, the process of ordaining a WD with a strong magnetic field is still debated. The current hypotheses for magnetic field generation all imply that some post-common envelope binaries should have highly magnetic WDs, but no young, detached binary with a highly magnetic WD has been observed. The model proposed by Schreiber et al. (2021) does not suffer from this problem. As WDs cool, their interior ions crystallize. This happens when Coulomb forces between electrons and ions overwhelm the kinetic energy of each particle (Hansen et al., 2004). As a result, the heavier oxygen continues to sink towards the core, while the

lighter carbon remains above. With the addition of convection by Rayleigh-Taylor instability (material bubbling up between layers) in the carbon layer, this difference in density is enough to result in a dynamo capable of generating field strengths up to a few hundred MG.

1.4 AR Sco: the first white dwarf pulsar

AR Sco was identified in 1971 as a δ Scuti type variable star (Satyvaldiev, 1971). Its period, 3.56 hours, falls within the normal pulsation range for that kind of variable, making it easy to misidentify. Marsh et al. (2016) are the first to report that AR Sco is actually a binary system consisting of a rapidly-spinning WD and an M dwarf (MD) companion. Interestingly, it exhibits short-period pulsations at 1.95 minutes, the WD spin period, and 1.97 minutes, the beat period between the WD spin and orbital periods. A beat period, qualitatively, is the result of combining two periodic signals of different frequencies that constructively and destructively interfere to form a new signal. For AR Sco, this is when one of the WD's magnetic poles comes to face the companion once again. AR Sco's variation is observable in radio, IR, optical, UV, and X-ray wavelengths (Marsh et al., 2016; Takata et al., 2018). It should be noted, however, that pulsed emission at the WD spin period hasn't been observed in the X-ray.

AR Sco is a pole-on rotator, meaning its spin axis is about 90 degrees from its magnetic axis (Geng et al., 2016; Garnavich et al., 2019). As can be seen in Figure 1 of Geng et al. (2016), the magnetic poles of the WD in AR Sco sweep across the surface of the MD twice with each rotation. This is evident in the light curve of the system, in which there are two pulses within one spin of the WD (Geng et al., 2016). The exact mechanism behind the emission is uncertain (Geng et al., 2016; Katz, 2017; Garnavich et al., 2019; Singh et al., 2021). The pulsed IR through UV emission is thought to be a result of irradiation of the companion. Based on velocity measurements the UV and optical line emission is coming from the side of the companion facing the WD (Marsh et al., 2016). Only during the pulse minimum then could we

possibly observe the WD in UV.

The WD in the system is highly magnetized; Buckley et al. (2017) suggest on the order of 100 MG. An electron-positron beam emanating from open field line regions creates a bow shock around the MD as it meets with the opposing stellar wind from the MD. Geng et al. (2016) propose that the bow shock is the source of synchrotron-emitting, relativistic electrons that cascade down onto the WD. However, Garnavich et al. (2019) provide a model in which magnetic reconnection between the WD's and MD's magnetic fields is responsible for accelerating those electrons. Their model would provide an explanation for the observed heating on the side of the MD that faces the WD. Whatever the source of the accelerated particles, synchrotron emission easily explains the radio and x-ray light from AR Sco (see Figure 1.1) (Geng et al., 2016).

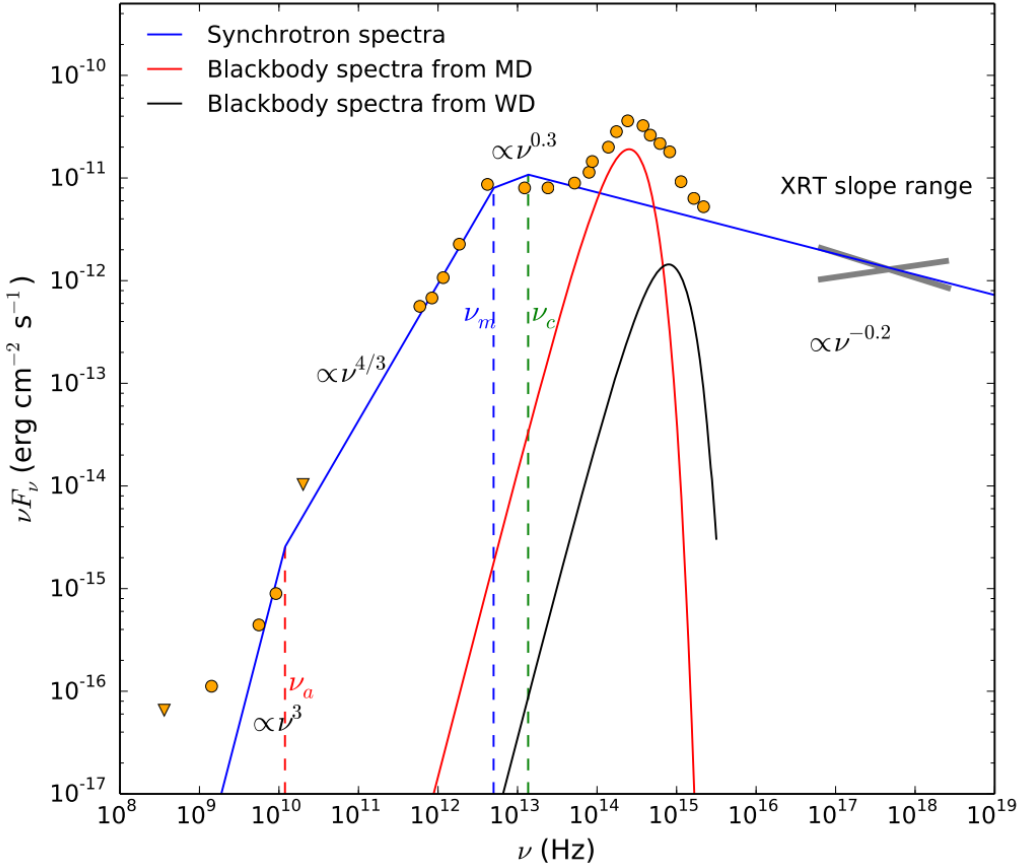


Figure 1.1: The spectral energy distribution of AR Sco, provided by Geng et al. (2016), along with blackbody models for the MD and WD, and a synchrotron model.

The exact strength of the WD’s magnetic field is contested. While polarization measurements by Buckley et al. (2017) indicate the field should be a few hundred MG, Lyutikov et al. (2020) propose a value around 10^5 G. Models of polar CV evolution show that it is possible to generate fields of up to 200 MG during the spin-up phase of the WD (Schreiber et al., 2021), so a high magnetic field strength should not yet be discounted for AR Sco.

To the knowledge of the author at the time of writing, there are no other twins of AR Sco and there is only one suggested candidate in the literature, ZTF18abnbzvx (Kato & Kojiguchi, 2021). To understand their evolution, population size, and CV evolution more broadly, it is important that we discover more systems like it. In this work, I will present a possible method of finding more such binaries and the tentative candidates for twins of AR Sco (although there is scant evidence on each of them). The method is discussed in the following chapter.

1.5 The origin of bright radio sources in our galaxy

Tetarenko et al. (2016)s suggest VLA J213002.08+120904 (hereafter VLA J2130+12) could be the first quiescent black hole X-ray binary (BHXB) found outside of a globular cluster and the first BHXB found via radio observations. With this one detection they estimate there are between 2.6×10^4 and 1.7×10^8 systems like it in our Galaxy at the $3\text{-}\sigma$ level. They point out that their lower limit just grazes the upper limit generated through population synthesis models.

With this uncomfortable circumstance, one may begin to think that this is indeed not a BHXB, but some other oddly bright radio source. To explain this lalth of unknown objects within our Galaxy, I can look elsewhere to known types of systems in our galaxy such as AR Sco or AE Aqr and its candidate twin, LAMOST J024048.51+195226.9 (Pretorius et al., 2021). The latter class is another moderately magnetized CV that is thought to be a propeller system, one in which the WD flings material that would be accreted outside of the

binary (Wynn et al., 1997). They are also radio sources (Bookbinder & Lamb, 1987; Pretorius et al., 2021). AE Aqr, AR Sco, and VLA J2130+12 are shown in Figure 1.2. All three are in the bottom left corner of the diagram, among the X-ray/radio quiet sources.

It is reasonable to say that since VLA J2130+12 has a radio luminosity an order of magnitude higher and is at most has an X-ray luminosity an order of magnitude lower, that it is not a binary like AE Aqr and AR Sco.

VLA J2130+12 has a radio/X-ray luminosity at least 100 times that of AE Aqr and AR Sco, suggesting it is a different class of object. However, since we know of very little systems like AE Aqr or AR Sco, we do not know the full range of luminosities they should have at various wavelengths. So with that in mind, we should not discount the possibility that WD/red dwarf binaries occupy this area of the plane.

Part of this thesis will be spent on estimating the population of AR Sco twins in the Galaxy (Chapter 4). This will then be compared with the estimate for systems like VLA J2130+12 (Section 4.3) so we can further discuss the possibility that the number of radio sources can be explained at least in part by AR Sco-like binaries.

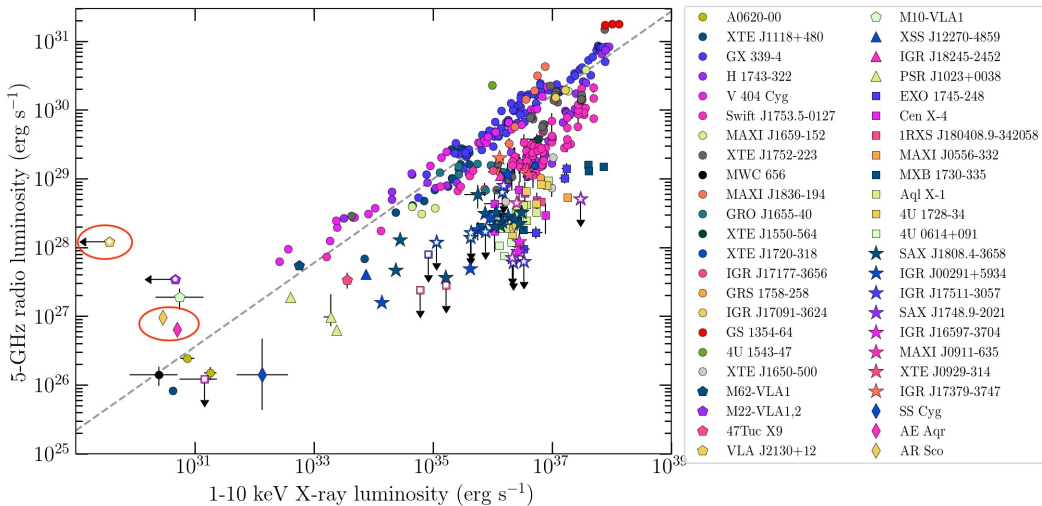


Figure 1.2: The $L_X - L_R$ plane of BHXBs, LMXBs, MSPs, and the CVs AR Sco and AE Aqr. The red circles show the objects of interest. This diagram was produced by Bahramian et al. (2018).

Chapter 2

Analyzing δ Scutis from ASAS-SN

AR Sco was first labelled a δ Scuti, so I suspect there may be other AR Sco twins misidentified now as δ Scutis. I will examine large optical surveys for variable stars and in this chapter I study data from the All-sky Automated Survey for Supernovae (ASAS-SN). I will cover the main method for finding AR Sco twins. I select the stars by luminosity and color before crossmatching them with radio and X-ray catalogs since AR Sco is a significant source of both wavelengths, but δ Scutis are not. I made attempts at finding periodic signals in ASAS-SN light curve data, but was unsuccessful. This chapter concludes with a list of 5 possible candidates.

2.1 The dataset

I took the sample from the ASAS-SN catalog of variable stars (Kochanek et al., 2017; Shappee et al., 2014). ASAS-SN is a multi-telescope survey that scans the sky down to a magnitude of ~ 17 , but saturates at $\sim 10 - 11$ mag. The cadence of observations is 2 - 3 days (Jayasinghe et al., 2018, 2019).

The full table downloaded from the ASAS-SN light curve database has 666,502 rows (the last download was in August 2021). I crossmatched this catalog with 2MASS to obtain the J and K magnitudes as well as the quality flags Q, R, C, X, and “extKey.” Doing this excluded stars with a bad photometry for a given magnitude (Q, R), prevented confusion between sources

Table 2.1: Objects with these flags were excluded from the final sample.

Flag	Value (s) excluded
Q	D, E, F, U
R	0
C	b, c, d, p, s
X	2
extKey	1

(C), and excluded entries in the catalog that might be extended sources (X, extKey). The exact values of each flag that were used to exclude candidates from the final sample are listed in Table 2.1. Since AR Sco was previously classified as a δ Scuti star, I included those, high-amplitude δ Scutis, and other uncertain classifications in the catalog: uncertain rotational variables, Mira variables, RR Lyrae Type AB variables, G Cas variables, and those without a confident classification. We crossmatched this set with Gaia to obtain the distances as well as the magnitudes for each. The length of this set used for the rest of the analysis was 55,657 rows.

2.2 Candidate selection with luminosity and color

Two selections for luminosity and color are described below. The variables common to both categories (shown in Figures 2.1 and 2.2) were analyzed in the next step, Section 3.

2.2.1 δ Scuti Period Luminosity Relation

To select for low luminosity variables, I plotted the Wesenheit (W_{JK}) magnitude against the period ($\log P$), recreating Figure 3 in Jayasinghe et al. (2020). Wesenheit magnitudes of any kind are constructed to be reddening free. At large distances this may not hold, given that they assume a particular reddening law. For any relation that uses a Wesenheit magnitude, the equation will have the same form as one using the intrinsic magnitude, but the two will be related by a constant. As shown in Madore (1982),

$$W = V - R(B - V), \quad (2.1)$$

where W is the Wesenheit magnitude, R is the ratio of total to selective absorption, V is the redder magnitude band, and B is the bluer magnitude band. Next, I need to expand these terms into their intrinsic values and color excess.

$$W = V_0 + A_\nu - R(B - V)_0 - R \cdot E(B - V). \quad (2.2)$$

The extinction, A_ν , and $R \cdot E(B - V)$ are equivalent.

$$W = V_0 - R(B - V)_0. \quad (2.3)$$

Thus, the Wesenheit magnitude is the same value, regardless of reddening. This makes it useful for the rest of the analysis, given the sources in ASAS-SN are spread throughout the Galaxy, some at long distances. The first Wesenheit magnitude (an absolute magnitude) that I will use is W_{JK} , defined by the following equation using 2MASS J and K,

$$W_{JK} = M_K - 0.686(J - K). \quad (2.4)$$

We will be using this equation for constructing the period-luminosity relation (PLR). For some variable stars, their period is closely tied to their luminosity, as with δ Scutis and can be represented as a simple linear equation. The PLR for δ Scutis (Figure 2.1) can clearly be seen in the rough line extending from $\log P \approx -1.3$ to 0.7. AR Sco lies below this line and so I selected stars in that area as well (indicated by the red, dashed lines). It seemed reasonable to use the distance underneath the theoretical PLR that Jayasinghe et al. (2020) used to discard quite a number of sources from their sample. The equation they use for the fundamental mode δ Scutis is

$$W_{JK} = -3.495 \log_{10}(P/0.1d) + 0.767, \quad (2.5)$$

and the perpendicular distance they chose is 0.11. While this sample is likely to contain γ Dor stars (Jayasinghe et al., 2020), it still has the possibility of holding some AR Sco twins and I accepted this contamination.

2.2.2 Gaia color magnitude diagram

Here, I recreated Figure 7 of Jayasinghe et al. (2019a) for our sample. This time Gaia color (Riello et al., 2021; Gaia Collaboration et al., 2016) is on the x axis and plotted against W_{RP} ,

$$W_{RP} = M_{G_{RP}} - 1.3(G_{BP} - G_{RP}) \quad (2.6)$$

In order to gather up those that are blue-ward of the “main sequence”, I made a cut at $G_{BP} - G_{RP} \approx 0.6$ and the line,

$$W_{RP} = 0.75 \log_{10} P + 3.5, \quad (2.7)$$

which was set by eye. We recognize this may carry with it some error, given the human eye is not infallible. However, I attempted to be generous with our selection. The main population in this data follows an approximate sideways

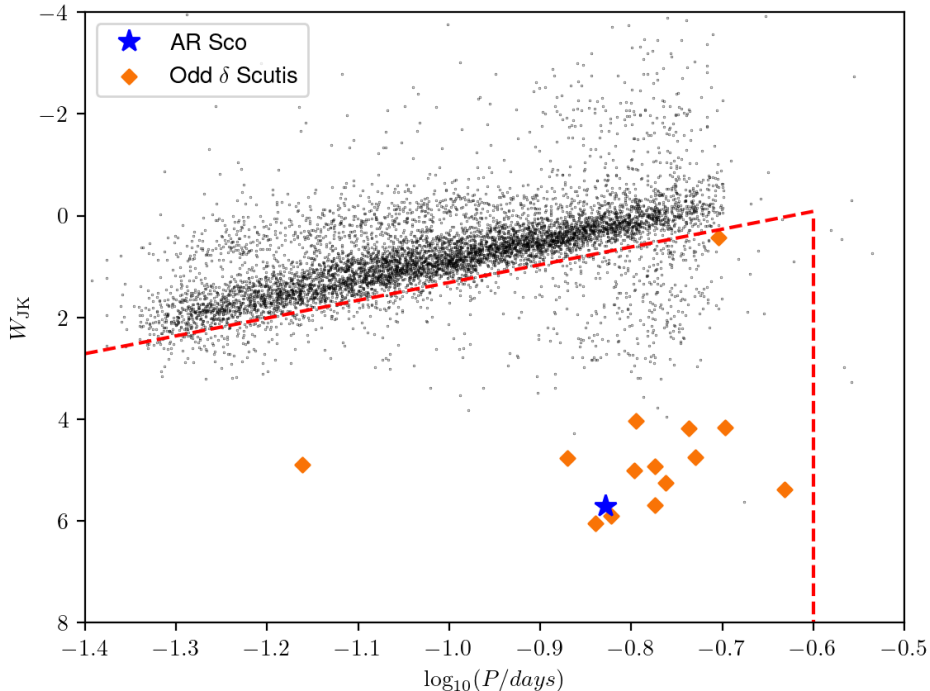


Figure 2.1: The PLR for δ Scutis. The black dots represent all the stars in our sample. Highlighted are the possible candidates, which appeared in the selections described in Section 2.2.

U (that is much more apparent in Jayasinghe et al. (2019a), Figure 7) from $W_{RP} = 0$ to $W_{RP} = 4$. All of our sources from this selection are blue-ward of the U, near the position of AR Sco. As you can see, one of the possible candidates in Figure 2.2 is nearly inside the main clump of stars ($G_{BP} - G_{RP} = 0.3$, $W_{RP} = 0.5$). This one is unlikely to be a good candidate, but it was still left in the final list because of its placement in Figure 2.1.

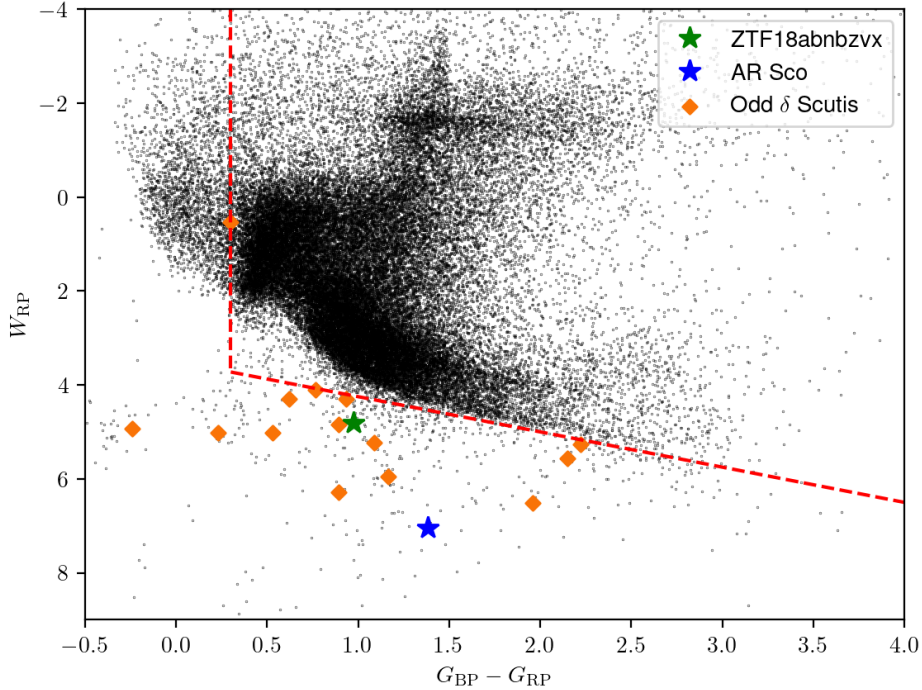


Figure 2.2: This is the CMD for our sample. All of the possible candidates are highlighted. These were also found to be dim in comparison to the other stars (see Figure 2.1). In the top right, there is slight right angle due to the horizontal branch.

The highlighted points from both Figure 2.1 and 2.2 are shown in Table 2.2 Most of these are either classified as high-amplitude δ Scutis or uncertain δ Scutis, but some were in the generic variable category. This is unsurprising as the other classifications are unlikely to be in the same position on the PLR. It is possible these could be at any point in the PLR since ASAS-SN could not conclusively categorize these.

2.3 Power spectra

Every one of the ASAS-SN light curves for the possible candidates was run through a variation of a Fourier transform, called the Lomb-Scargle method. This method is one that allows for uneven sampling of data, unlike regular Fourier transforms. The code that processed the light curve data was from AstroPy (Astropy Collaboration et al., 2018). While the cadence of the ASAS-SN light curves was not enough to pick out a confident signal at around a few minutes (which would be strong evidence for an AR Sco twin), the goal of this step was simply to see if the “fuzz” on each light curve was high enough to create a small peak. What we would want to see is a spike that rises above the noise near 1.5×10^{-4} days (13 seconds), since there would almost certainly be plenty of frequencies that over-fit the data. None of the power spectra were particularly interesting, but there are a couple of examples below. In hindsight, this is not surprising as I was trying to find a signal greater than the Nyquist frequency given the space between observations.

The horizontal lines in both diagrams are the 1%, 5%, and 10% false alarm probabilities. This is the probability that a peak above the line has fit the data by random chance.

2.4 Looking for radio and X-ray counterparts

A crucial step in deciding whether an object is a good AR Sco candidate is whether it has a radio or X-ray counterpart. Thus, I submitted the coordinates from Table 2.2 to HEASARC and CIRADA cutouts to search for X-ray and radio counterparts respectively. The HEASARC archive¹ offers a multitude of UV and X-ray catalogs. We specifically queried the X-ray observatories *Chandra*, *XMM Newton*, *Swift*, and ROSAT, choosing the default search radius for each mission. These had sufficient sensitivity and focusing ability. The Canadian Initiative for Radio Astronomy Data Analysis (CIRADA) provides cutouts² from selected radio and infrared missions. Here I selected cutouts

¹<https://heasarc.gsfc.nasa.gov/W3Browse/>

²cutouts.cirada.ca

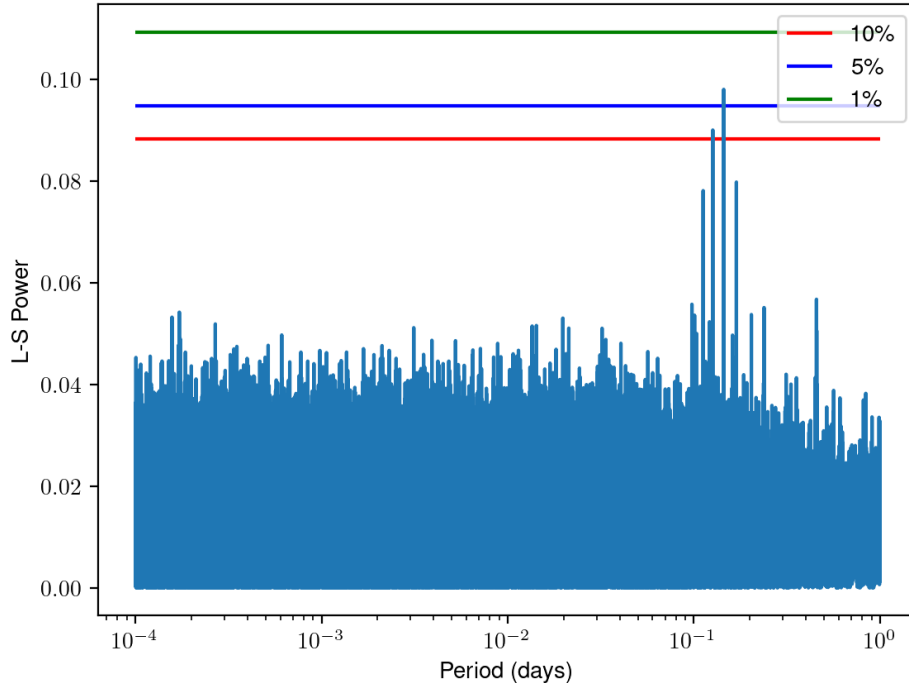


Figure 2.3: The power spectra for a candidate without peaks near a few minutes that are significantly above the noise.

from the radio catalogs VLASS-QL, FIRST, and NVSS. These catalogs were made using the Karl G. Jansky Very Large Array (VLA). The VLA is in the northern hemisphere so much of the southern sky cannot be covered by these catalogs (anything below ~ -40 deg declination is invisible to the VLA).

Unfortunately, I only saw obvious X-ray and radio counterparts for one of our targets, which turned out to be QS Vir, a known post-common envelope binary. This will be discussed in Section 2.5.1. In addition, I recovered the known CV, SW Sex. Based on these non-detections of the rest of the sample, I can use archival survey data to find a limit on the luminosity in each band. For X-ray, it would be reasonable to choose the ROSAT All-Sky Survey (RASS; Voges et al., 1999). despite its age. RASS scanned the whole sky from 0.1 - 2.4 keV between 1990 and 1991, but due to the coverage it is a good choice use when calculating this limit. The flux limit quoted in the updated 2RXS catalog (Second RASS source catalog) is $10^{-13} \text{erg s}^{-1} \text{cm}^{-2}$ (Boller et al., 2016).

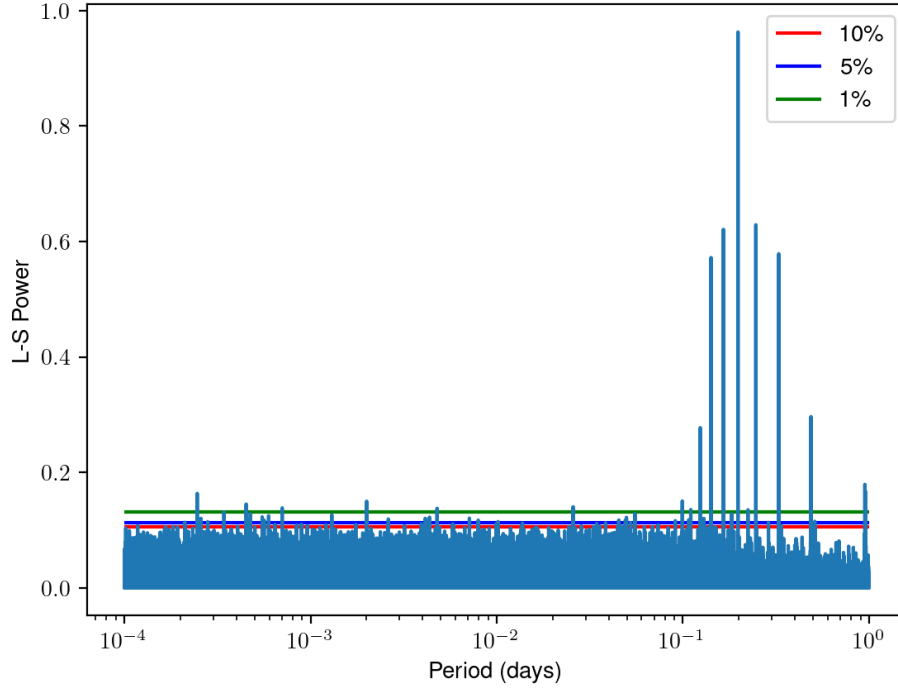


Figure 2.4: The power spectra for a candidate with peaks near a few minutes that reach above the 1% false alarm probability. They are not significantly above the noise however.

The VLA Sky Survey (VLASS) is a mission to map the sky in the range 2 - 4 GHz that began in 2017 (Lacy et al., 2020). The typical rms noise in VLASS images $120\mu\text{Jy}$ (Lacy et al., 2020), but at most $200\mu\text{Jy}$ (G. Sivakoff, 2020, priv. comm.). This latter value was multiplied by 5 to simulate a confident $5\text{-}\sigma$ detection limit of 1 mJy .

The X-ray luminosity was calculated with,

$$L_{X,lim} = 10^{-13} \text{ erg s}^{-1} \text{ cm}^{-2} \cdot 4\pi d^2. \quad (2.8)$$

This will return the upper limit on the brightness based off of ROSAT's sensitivity. As for the radio luminosity,

$$L_{R,lim} = 1\mu\text{Jy} \cdot 3\text{GHz} \cdot 10^{-23} \text{ erg Jy}^{-1} \cdot 4\pi d^2, \quad (2.9)$$

where 3 GHz was included as it is the middle of the frequency range for the

VLA. For reference, AR Sco’s X-ray luminosity is 4.9×10^{30} and its radio luminosity is 1.8×10^{26} at 1.4 GHz. We determined that since this is the same order of magnitude as for $L_{R,lim}$, it is a reasonable comparison.

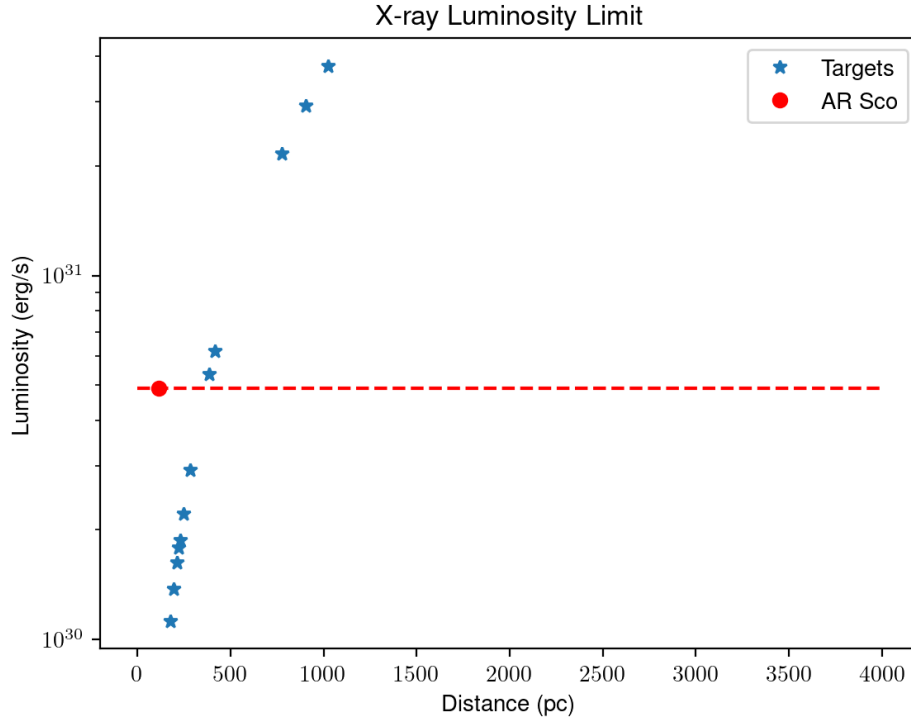


Figure 2.5: The X-ray luminosity limit of each possible candidate based on the limiting flux of ROSAT.

The luminosity limits are shown in Figures 2.5 and 2.6. The red star and line represent the level of AR Sco’s distance and luminosity. For clarity, the position at which AR Sco would have to be in order to just pass the 2RXS flux limit is 370 pc. For VLASS, that value changes to 230 pc. These upper limits on the luminosity are useful for determining whether I have enough information to rule out any of the possible candidates. If the upper limit on the luminosity is above that for AR Sco (or equivalently the distance is farther than the limiting distance), I can conclude there is not enough information to rule it out as a possible candidate. We would need to ask for time on an X-ray or radio telescope rather than using archival data. Those that are below the line, by comparison, can be ruled out as X-ray and radio sources and therefore

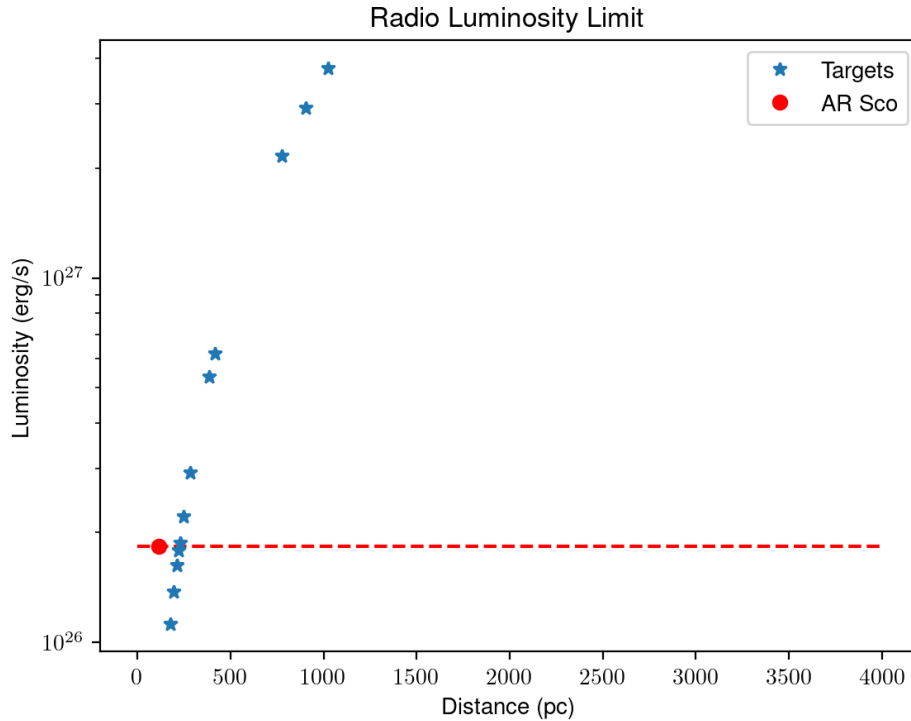


Figure 2.6: The 3GHz radio luminosity limit of each possible candidate based on the typical noise in VLASS.

are not good candidates for AR Sco twins.

2.5 Discussion

The final 5 possible candidates that were blue and dim are listed in Table 2.2 above the dashed line. Only high-amplitude δ Scutis and uncertain δ Scutis were left after both selections. Any star below the red line in Figure 2.5 was discarded as a possible candidate. The reason I chose this limit is because the X-ray luminosity limit was more stringent than the radio. The result is that the stars in Table 2.2 were both undetected by ROSAT and undetected by the VLA. They are far enough away that they would require a longer exposure time from both observatories. To rule any of these possible candidates out in the future follow-up in X-ray and radio is necessary. It is also important that short-cadence time-series optical data be obtained as well. Since AR Sco's spin and beat period are both around 2 minutes, a cadence of less than a minute

Table 2.2: The results from the selection on the PLR and CMD. The 4th column shows the category of each source in the ASAS-SN variable star catalog. DSCT: is an “uncertain δ Scuti,” HADS is a “high-amplitude δ Scuti,” and VAR is a generic variable category. The list of possible candidates from ASAS-SN after accounting for the radio and X-ray luminosity limits are above the dashed line. The coordinates and distances are taken from Gaia EDR3 (Gaia Collaboration et al., 2021; Riello et al., 2021) and rounded to the nearest arcsecond.

RA (deg)	Dec (deg)	Distance (pc)	ASAS-SN Type
97.5023	-71.8940	900 $^{+20}_{-20}$	DSCT:
134.4243	-11.0574	420 $^{+40}_{-40}$	HADS
220.4094	56.4381	1025 $^{+16}_{-17}$	HADS
300.7812	-43.7634	390 $^{+50}_{-30}$	DSCT:
314.4374	3.3681	780 $^{+200}_{-100}$	DSCT:
117.5629	49.7258	213 $^{+2}_{-2}$	DSCT:
150.1267	0.0645	177 $^{+2}_{-1}$	VAR
153.7890	-3.1425	602 $^{+14}_{-10}$	DSCT:
160.7989	-44.5487	250 $^{+30}_{-20}$	DSCT:
207.4669	-13.2269	50.1 $^{+0.07}_{-0.06}$	DSCT:
237.6802	-57.8210	230 $^{+50}_{-30}$	VAR
272.9130	-68.1129	220 $^{+40}_{-30}$	HADS
296.7856	-38.6199	200 $^{+30}_{-30}$	DSCT:
297.8948	-22.7951	290 $^{+30}_{-30}$	DSCT:

would be required by Nyquist’s theorem.

Among the group that could be ruled out (below the dashed line), the source at RA = 272.9130, Dec = -68.1129 was clearly not a δ Scuti. The light curve has a wide peak and narrow trough, characteristic of a W UMa, an eclipsing common-envelope binary. In AAVSO VSX catalog (Watson et al., 2006), this same star is categorized as a W UMa with double the period quoted in ASAS-SN (0.337 days vs 0.168 days). It is likely that the troughs were a similar enough magnitude for the ASAS-SN pipeline to be confused. As with the discovery of CVs in our dataset, it is also encouraging to see another type of binary system in a catalog of δ Scutis.

2.5.1 CVs in ASAS-SN

In the list below the dashed line of Table 2.2, I recovered two known systems: QS Vir and SW Sex. The former is a low-accretion rate CV and the latter is a non-magnetic CV. They are both labelled as uncertain δ Scutis in the ASAS-SN variable star catalog. While these are certainly not AR Sco twins, it is encouraging to see that through the method described in this chapter, I can recover binary systems that contain a white dwarf and late-type stars.

While checking for radio counterparts of the preliminary list, QS Vir appeared as a point source in VLASS-QL. From the cutout image provided by CIRADA, the flux is $980 \pm 160 \mu\text{Jy}$ at RA = 207.466917, Dec = -13.226739, MJD 58598.28 (G. Sivakoff & A. Hughes, 2021, priv. comm.). QS Vir is also in the XMM Serendipitous Source Catalog (Webb et al., 2020). Its X-ray luminosity is $5.0 \times 10^{29} \pm 8.3 \times 10^{27} \text{ ergs}^{-1}$. At the time of writing, there is no known reported radio counterpart to QS Vir in the literature. As the radio study of CVs is relatively new, I believe this result will be useful to the scientific community.

2.6 The importance of accurate distances

It should be noted that with the updated distances from Bailer-Jones et al. (2021) (based on the parallaxes of Gaia Collaboration et al. (2021)), our original list of candidates that used Bailer-Jones et al. (2018) (based on the parallaxes of Gaia Collaboration et al. (2018)) changed significantly. For example, the distance for one star at RA = 146.251, Dec = -38.0889 increased from 231 pc to 3448 pc, which inevitably took it out of the regions in Figures 2.1 and 2.2 defined by the red lines. We chose to use all distances from Bailer-Jones et al. (2021) since it is the most up to date.

Before the update, one of the targets (RA = 180.395, Dec = -1.8208)) appeared to have a signal near minute-scale in its periodogram. As such, I asked for time on Swift (Target ID 14133) (Burrows et al., 2000, 2005). The X-ray telescope on board Swift observes from 0.2-10 keV and provides 1-3 arcsecond position accuracy. If the number of counts are sufficient, Swift

also produces spectra with 140 eV resolution at 6 eV (at launch in 2005). Unfortunately, our observations showed no detection at the coordinates for this possible candidate. The exposure time was 2 ks, which would predict around 5 counts if it were indeed around the same luminosity as AR Sco.

Chapter 3

Other searches for candidates

Searching more than one catalog is necessary to find AR Sco twins. Here I apply the method from the previous chapter to other catalogs of δ Scutis. I do not perform the short period search from Section 2.3. In addition, I also attempt a similar method of finding candidates in Gaia only involving a CMD selection and amplitude.

3.1 Rodríguez et al. (2000) Catalog

The review paper Rodríguez et al. (2000) gathered all the known δ Scutis at the time: 636 in total. The catalog is an amalgam of sources found in other catalogs (including Hipparcos and MACHO). This included AR Sco as it was then classified as a δ Scuti.

In order to use the method outlined in Chapter 2 on this sample, cross-matching became an immediate issue; the overwhelming majority of this catalog no longer has coordinates accurate to within an arcsecond (see Figure 3.1). For a trustworthy crossmatch, I searched for the reported names of the stars and downloaded their positions from Simbad¹. However, there were 224 unnamed sources that I had to use a different method to find. We made a 30'' cone search around each of the original coordinates. To make sure I found the correct star, I also employed a 0.5 mag limit on how different the V magnitude should be between Simbad and Rodríguez et al. (2000). In some cases, there were a lot of repeats for the same cone search (e.g. one source was in a cluster).

¹simbad.u-strasbg.fr/

We chose the closest match when this happened.

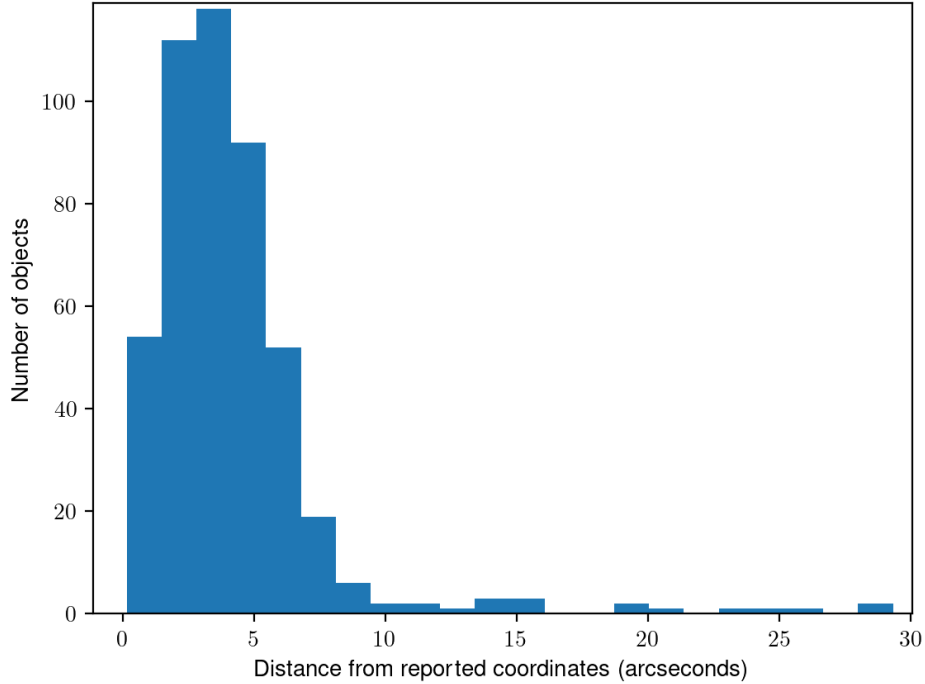


Figure 3.1: A zoomed-in look at the distance sources in Rodríguez et al. (2000) were from their current Gaia EDR3 coordinates (Gaia Collaboration et al., 2021; Riello et al., 2021). They are typically within 5 arcseconds, but there were a handful beyond an arcminute.

Only three of the stars in this catalog appeared in the regions of the CMD and PLR that I outlined in Chapter 2, including AR Sco (the highlighted star near the bottoms of Figures 3.2 and 3.3). These also did not have a visible X-ray or radio counterpart when I queried HEASARC and the CIRADA cutouts. However, the one above the dashed line in Table 3.1 could not be ruled out as a possible candidate because it is far enough away that it would not appear in RASS. It is a reasonable proof of concept that AR Sco was able to pass through our selections. The other two that appear highlighted are fairly close to the main group of stars by comparison and should not be taken as incredibly confident candidates.

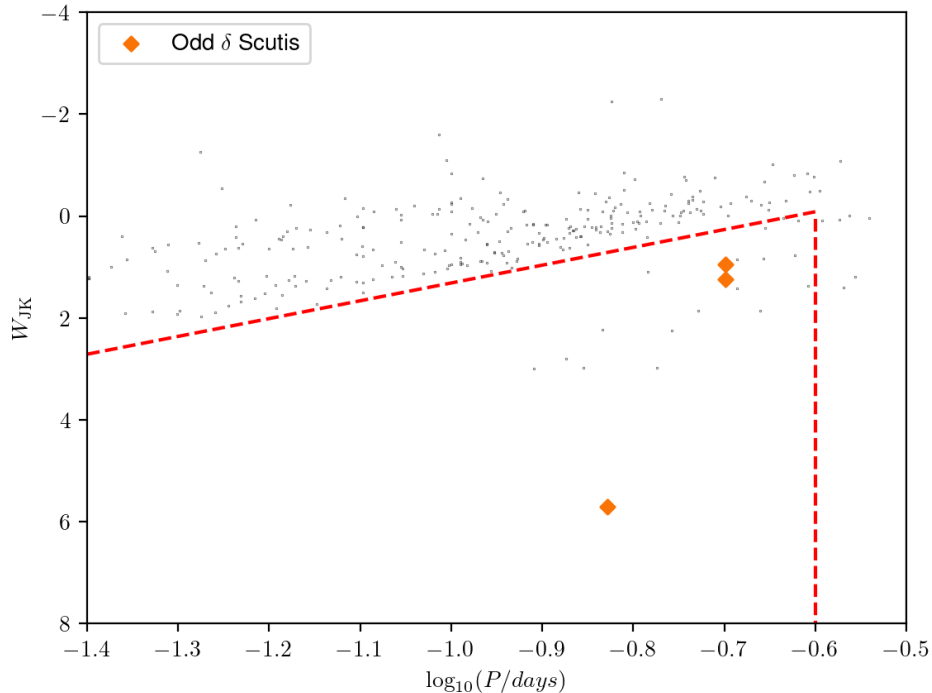


Figure 3.2: The PLR for Rodríguez et al. (2000) δ Scutis with the odd sources highlighted. AR Sco is the lowest luminosity of the three.

3.2 The Zwicky Transient Facility

The largest catalog I searched by far was the Zwicky Transient Facility (ZTF). There are over 16,000 δ Scutis in their catalog, making it an ideal place to search for AR Sco twins. ZTF is run out of the Palomar 48 inch optical telescope and is the successor to the Palomar Transient Facility (Bellm et al., 2019). They use a machine learning algorithm (Mahabal et al., 2019) to classify the variable stars in their catalog. Their input to the algorithm includes

Table 3.1: The list of δ Scutis from Rodríguez et al. (2000) that appeared blue-ward of the main population and low luminosity except for AR Sco. The coordinates and distances are taken from Gaia EDR3 (Gaia Collaboration et al., 2021; Riello et al., 2021) and rounded to the nearest arcsecond.

RA (deg)	Dec (deg)	Distance (pc)
63.7537	-69.5367	663 ⁺⁵ ₋₆
238.6678	8.5803	79.75 ^{+0.14} _{-0.20}

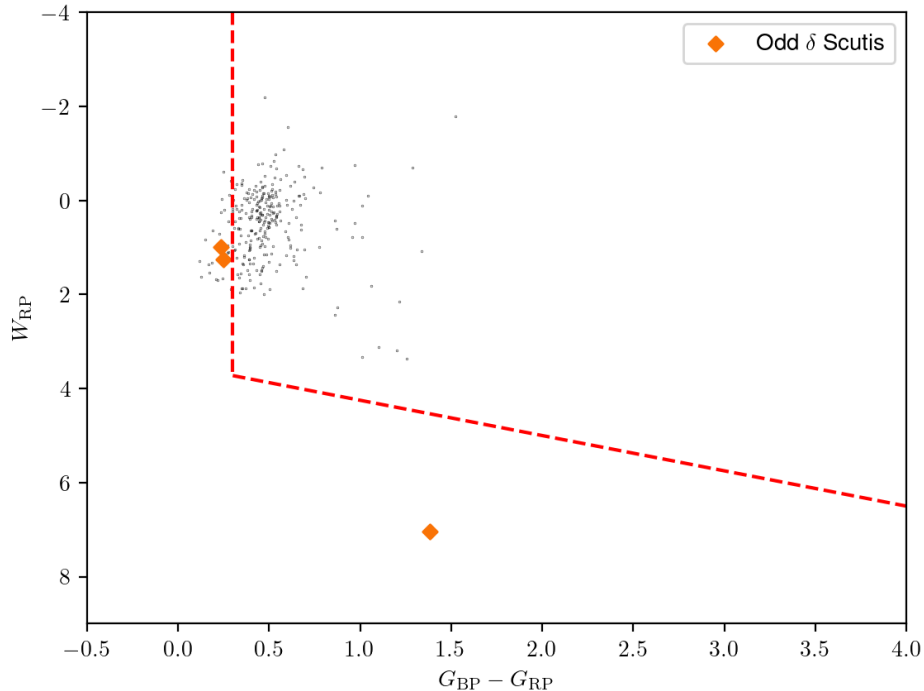


Figure 3.3: The CMD for Rodríguez et al. (2000) δ Scutis with the odd sources highlighted. AR Sco is the lowest luminosity of the three.

light curve statistics and the period extracted by the Lomb-Scargle method. Note that ellipsoidal variables (binary systems) have a 1.5% chance of being misclassified as δ Scutis (see Figure 5 in Richards et al. (2011)).

To search for possible candidates in this catalog, I ran their data through the same series of tests as I did for ASAS-SN. We retained the 8831 sources present in 2MASS. After selecting those that were blue and dim for their period (see Section 2.2), I was left with 23 “odd” sources. None of these appeared in a search with CIRADA, but a few appeared to be X-ray sources. For those that did not have an X-ray counterpart, I produced the luminosity limit plots as before.

Crossmatching with HEASARC also revealed that there is contamination here from CVs. Before excluding the poor photometry in 2MASS, EU UMa was part of our sample. This is a polar CV (an AM Her system) with a period of 80 minutes and a visual magnitude of 17 (Mittaz et al., 1992; Ramsay et al.,

2004; Warner, 2003). No other CVs appeared in our final list, however.

The PLR and CMD for the ZTF samples are shown in Figures 3.4 and 3.5 respectively. The shape of each sample differs significantly from ASAS-SN. In the case of the PLR, there is a larger vertical spread that could possibly be due to the increased error in parallax at large distances, and larger distance sources are characteristic of ZTF (the distribution of ZTF sources peaks at ~ 4000 pc). Since we need to know the distance to each source in order to calculate W_{JK} , the result would be a spread in the data. The wider spread on the short period end of the PLR could also be the “overtone” population of δ Scutis that is much more apparent in the ASAS-SN data (Figure 2.1). Above the line defined by Equation 2.5, there is another PLR that defines the overtone mode δ Scutis. This population isn’t important for our analysis however. As for the CMD, the U shape shown in Figure 2.2 is lost, since there were only variables classified as δ Scutis in the ZTF sample, unlike the ASAS-SN sample that had uncertain rotational variables, Mira variables, RR Lyrae Type AB variables, G Cas variables, and those without a confident classification. In addition, the points are smeared towards the red end of the plot in Figure 3.5. Once again, this is likely due to large distances as reddening will increase along with it.

The more significant spread and thus larger sample of “odd” stars in our sample are highlighted by the red dashed lines, which are the cuts in the data. Although they are off the side of the plot, Figure 3.5 also included a couple of very bright and very red stars (near $G_{BP} - G_{RP} = 7$, $W_{RP} = 10$). Their position indicates that they are not δ Scutis, but mistakenly classified semi-regular or irregular variables.

The list of the preliminary 23 candidates are shown in Table 3.2 (above and below the dashed line). One of the original 23 that were classified as blue and dim by our method (RA = 18.17688, Dec = 58.46590) appeared to have a counterpart in the RASS Bright Source Catalog, 1RXS J011242.1+582748. Since RASS has an inadequate positional accuracy (12.7 arcseconds) to determine whether this X-ray source coincided with the coordinates for our δ Scuti, I obtained time on Swift (Target ID 14414). The count rate reported in

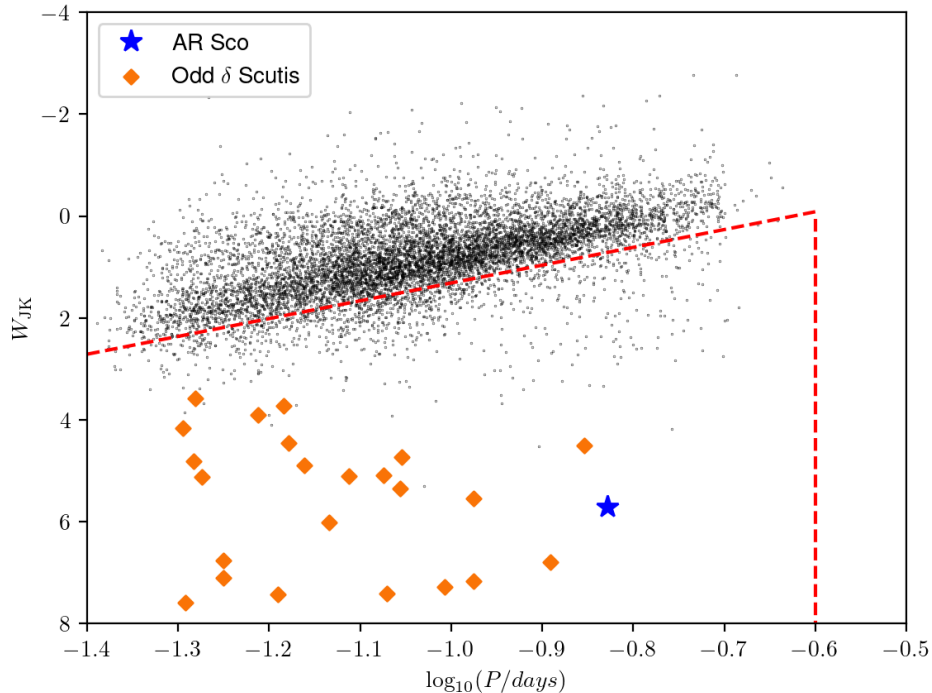


Figure 3.4: The PLR for ZTF δ Scutis with the odd sources highlighted.

RASS/BSC was 0.056 ct/s, translating to 0.13 ct/s for Swift. If the source had not dimmed, I expected roughly 130 counts in our 1 ks observation. However, there were no photons at that position in the X-ray image, but our δ Scuti was visible in UV at the coordinates from Gaia. The X-ray emission was probably a transient event that I cannot determine to be associated with the δ Scuti at our coordinates.

One of the stars in Table 3.2 appeared in the Swift 2SXPS catalog. Its Gaia EDR3 coordinates rounded to the nearest arcsecond are RA = 320.4077, Dec = 44.3732. The object, 2SXPS 169712 (Target ID: 49932), did not appear persistent, rather it faded over the course of a day and after a few days time, was not visible in X-rays at all. We extracted the X-ray source position as well as a light curve using the web interface provided by the UK Swift Data Science Center (Evans et al., 2007, 2009; Goad et al., 2007). The position is 320.40849, 44.373664 with a 90% confidence radius of 3.1". Inside the light curve, we see evidence of multiple flares from this object. Its flux in 2SXPS

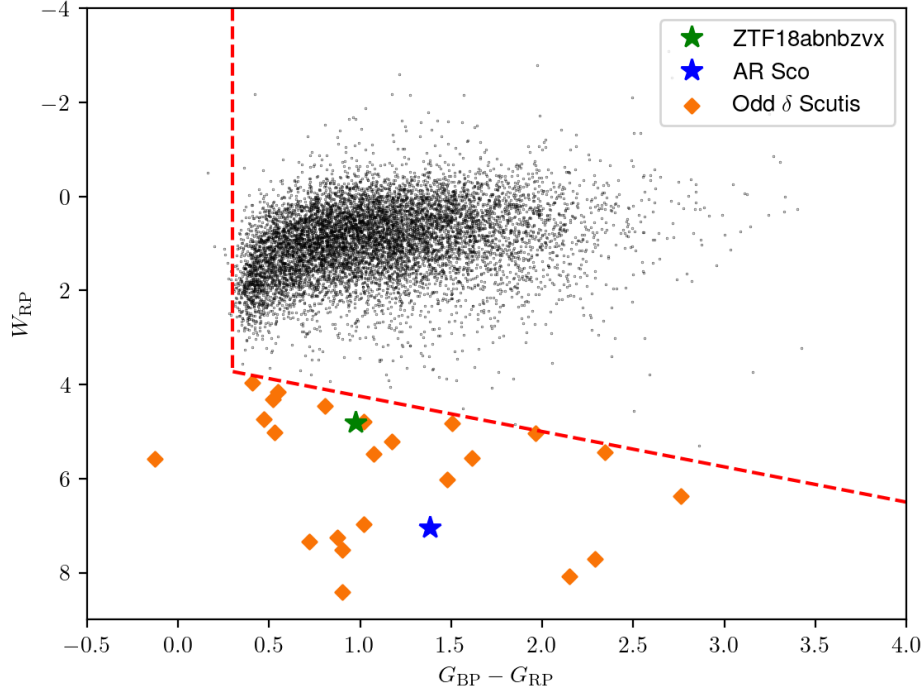


Figure 3.5: The CMD for ZTF δ Scutis with the odd sources highlighted.

is $1.60 \pm 0.16 \times 10^{-12} \text{ erg s}^{-1} \text{ cm}^{-2}$. The coordinates in the catalog are 4.4 arcseconds away from what I calculated, however. Since its distance is $\sim 301 \text{ pc}$, it can not be ruled out as a radio source from the VLASS flux limit. Pointed observations are necessary to rule it out as a possible candidate.

The final list of possible candidates from the ZTF catalog of δ Scutis are shown above the dashed line in Table 3.2. Since the X-ray luminosity was again the more stringent limit on what could be excluded, this was the limit I chose when presenting these 15 sources. Only those 14 were above the red line (representing AR Sco) in Figure 3.6 could not be ruled out as possible candidates. The one extra is our variable X-ray source (Figure 3.8), since it could not be ruled out based on its radio luminosity limit.

Table 3.2: The list of final candidates from the ZTF sample are above the dashed line. Those that could be ruled out based on their X-ray luminosity limits are below the dashed line. The coordinates and distances are taken from Gaia EDR3 (Gaia Collaboration et al., 2021; Riello et al., 2021) and rounded to the nearest arcsecond. The variable X-ray source is marked with an asterisk.

RA (deg)	Dec (deg)	Distance (pc)
42.2703	36.7306	980 $^{+140}_{-150}$
75.7609	58.0156	800 $^{+500}_{-200}$
60.8847	64.1870	450 $^{+70}_{-50}$
85.1401	14.7350	670 $^{+140}_{-120}$
88.1710	34.6892	700 $^{+180}_{-130}$
102.0577	12.6189	440 $^{+80}_{-70}$
144.3340	23.5996	2500 $^{+500}_{-400}$
267.3497	15.3990	1700 $^{+800}_{-700}$
284.8824	-9.5520	1200 $^{+500}_{-300}$
293.8854	27.6639	630 $^{+60}_{-70}$
298.1428	7.8479	1700 $^{+200}_{-200}$
314.4374	3.3681	780 $^{+200}_{-100}$
320.4077	44.3732	302 $^{+4}_{-5}$ *
338.0676	18.7007	1300 $^{+700}_{-400}$
346.6270	44.3135	616 $^{+10}_{-11}$
18.1769	58.4659	365 $^{+15}_{-12}$
47.0084	62.3171	111.4 $^{+0.8}_{-0.9}$
92.6162	5.9365	250 $^{+30}_{-30}$
281.5085	22.8812	139 $^{+13}_{-12}$
290.2606	65.0187	153 $^{+2}_{-2}$
297.1757	18.3476	190 $^{+50}_{-20}$
300.4260	26.6380	268 $^{+21}_{-18}$
352.4400	57.0292	370 $^{+30}_{-20}$

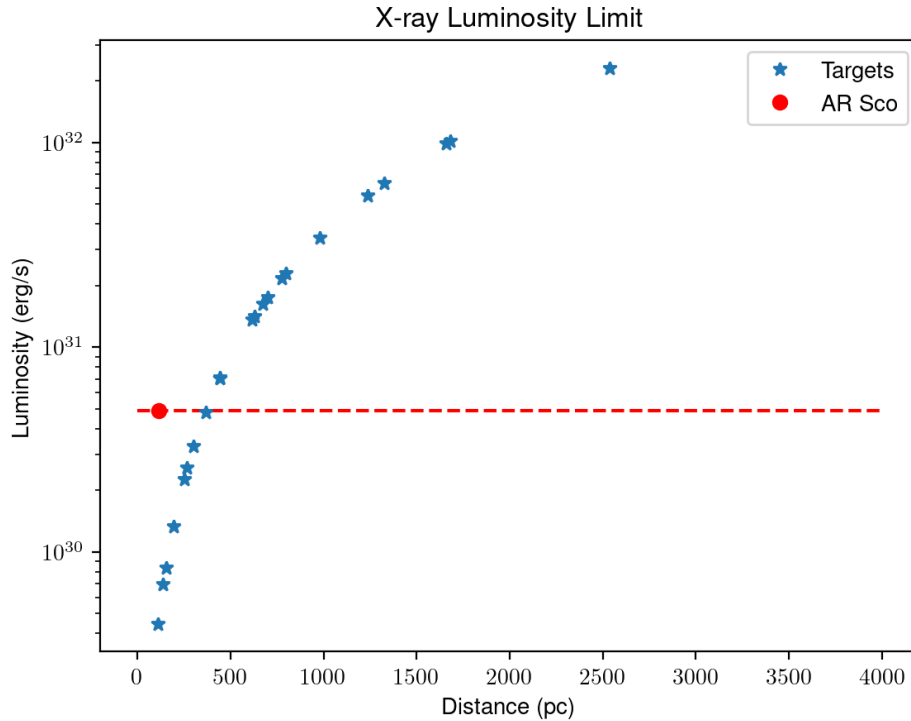


Figure 3.6: The X-ray luminosity limit for all the sources in Table 3.2. This was the more stringent limit, so I used this to exclude possible candidates.

3.3 Gaia

Gaia is a space-based telescope that measures the position of over a billion stars at high-accuracy in order to obtain parallax. Given the wealth of data it provides, Gaia has been used to classify numerous variable stars. The variables for this analysis were taken from Rimoldini et al. (2019) using the selection criteria from Appendix B in Gaia Collaboration et al. (2019). These put constraints on the error in magnitudes, the number of times the source was visible, the error in the parallax, and ensures the parallax was above 0 (negative parallaxes are unphysical). They categorized their stars using statistics of time-series data, except they did not use the frequency because the data were insufficient for a reliable Fourier decomposition. For context, Gaia observes using its Nominal Scaling Law (NSL). This means that the time between observing some region of the sky is variable, although the typical cadence is 20 to 40 days (Eyer et al., 2017).

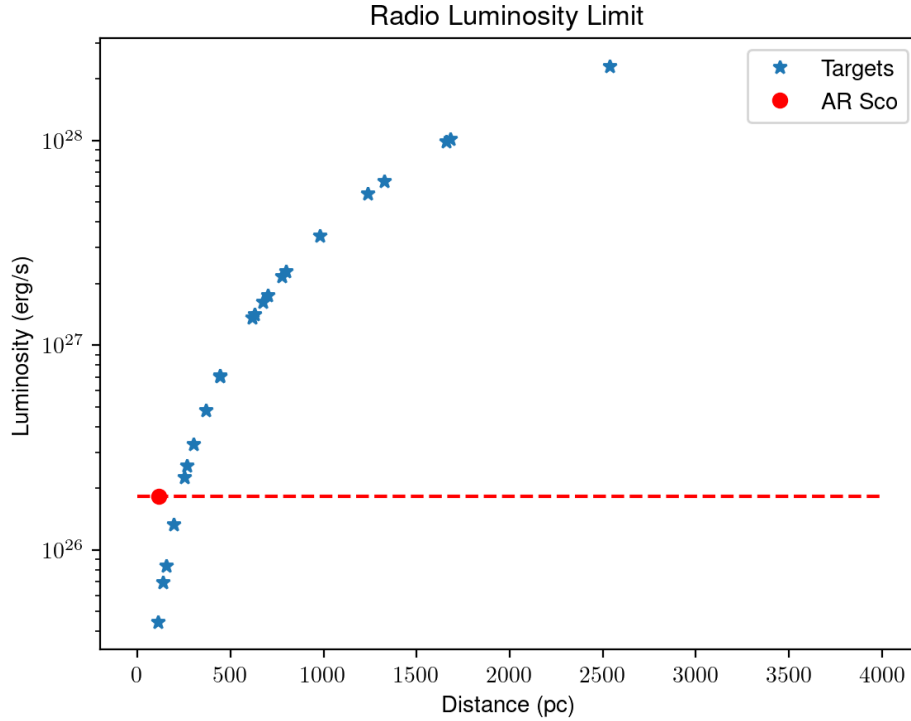


Figure 3.7: The 3 GHz radio luminosity limit for all the sources in Table 3.2.

The Gaia table `gaiadr2.vari_classifier_result` holds the information regarding the class of each source, while the statistics they used can be found in `gaiadr2.vari_time_series_statistics`. Both of these tables can be accessed through the Gaia data archive.² δ Scutis in this catalog are lumped in with SX Phoenicis stars, but this should not be a problem for our search. The distances were once again taken from Bailer-Jones et al. (2021).

In Rimoldini et al. (2019) Figure 7, there is a group of blue outliers in the group of δ Scutis around $G_{BP} - G_{RP} = 0.5$ and below G magnitude 2. Since these are more blue than the rest of the population, it seemed reasonable to investigate these as possible AR Sco twins. The sources I used are shown in Figure 3.9. The cut I made is defined by the following equation, which was set by eye.

²<https://gea.esac.esa.int/archive/>

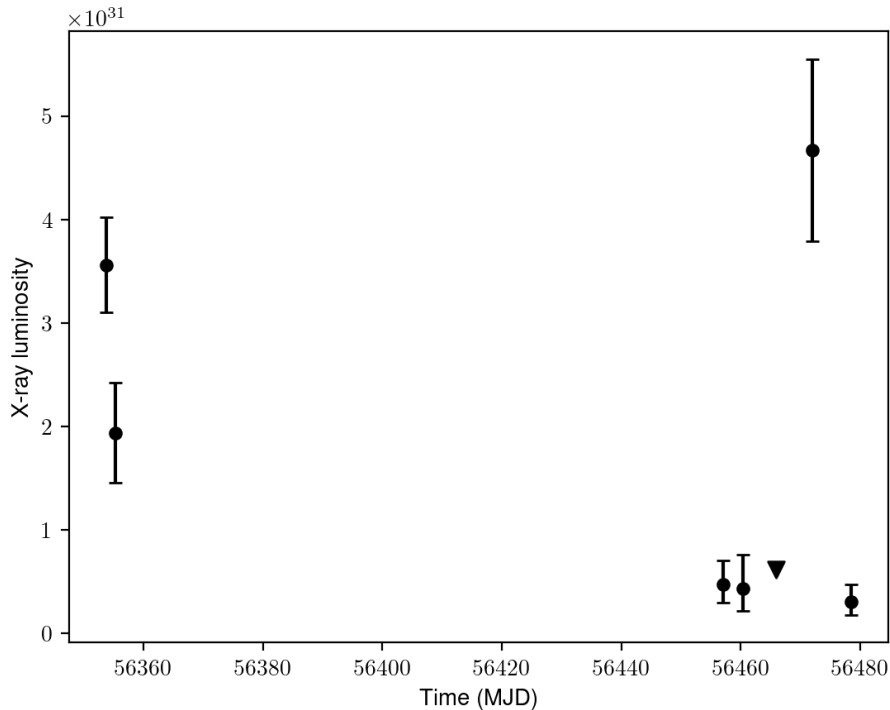


Figure 3.8: Swift XRT light curve (0.2 - 10 keV) for 2SXPS 169712, which is at 302^{+4}_{-5} pc (Gaia Collaboration et al., 2021). Here you can see the indication of two peaks at MJD = 56350 and 56470.

$$M_G = 2.66(G_{BP} - G_{RP}) + 3 \quad (3.1)$$

The group of red points in the figure are our selected sources to analyze further and the blue points are the ones that showed a result in HEASARC when I included *Chandra*, *XMM Newton*, *Swift*, and ROSAT. Some of these actually appear to have X-ray counterparts and could be confused with known or candidate CVs. It is also interesting that the CVs in Table 3.3 are included in Geier et al. (2019), which reports a list of hot subdwarfs (subluminous O or B stars) from Gaia. The authors selected their sample by imposing limits on colour and magnitude. Clearly, CVs in this region of the CMD can be confused with δ Scutis or other types of singular stars. Radial velocity measurements and pointed x-ray observations would be necessary to tell the difference.

While 3 of the 4 δ Scutis turned out to be known or candidate CVs (see

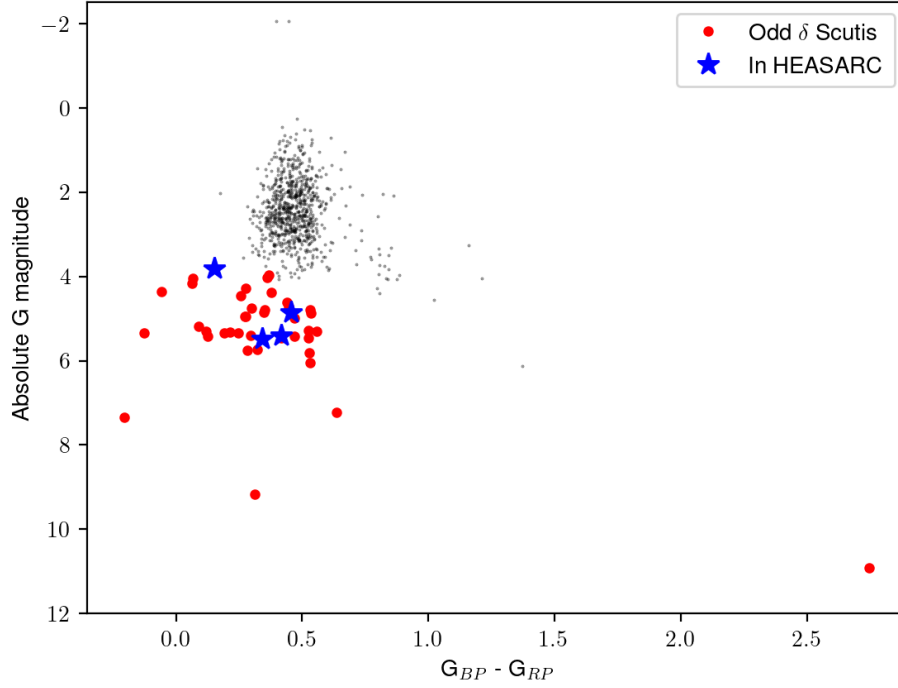


Figure 3.9: A recreation of part of Figure 7 from Rimoldini et al. (2019) to focus on δ Scutis. Red points are those that I selected to investigate. Blue points are those that showed up in our HEASARC query.

Table 3.3), one (XMMSL2 J185453.6-142834) appeared in the XMM slew survey with a flux of $1.62 \pm 0.79 \times 10^{12} \text{ erg s}^{-1} \text{ cm}^{-2}$. The Gaia EDR3 distance is $1320 \pm 60 \text{ pc}$, so the estimated X-ray luminosity is $\sim 3 \times 10^{32} \text{ erg s}^{-1}$ between 0.2 keV to 12 keV. With this in mind, we asked for 1 ks of time on Swift (Target ID 14404) to improve on the position and flux measurement (the slew survey has a 90% confidence radius of 11.3 arcseconds). However, after examining the observations there is no discernible X-ray source at these coordinates. We conclude that whatever was detected by XMM was a transient event. There is no counterpart in RASS as well, meaning that it is flux was at most $10^{-13} \text{ erg s}^{-1} \text{ cm}^{-2}$ before 28 March 2014. Given the distance to this object, it can still not be ruled out as an X-ray source unless one observes it with a longer exposure time (preferably over 3 ks if using Swift).

The majority of the red points in Figure 3.9 could not be ruled out. In

Table 3.3: The list of δ Scutis from Gaia that returned a result in HEASARC. The first, third, and fourth are known CVs. The coordinates are taken from Gaia EDR3 (Gaia Collaboration et al., 2021; Riello et al., 2021) and rounded to the nearest arcsecond.

Name	RA (deg)	Dec (deg)	Telescope(s)
V442 Oph	263.0630	-16.2561	Swift, XMM, ROSAT
XMMSL2 J185453.6-142834	283.7217	-14.4771	XMM
CP Lac	333.9212	55.6170	Swift, ROSAT
OR And	346.1560	49.4566	Swift, ROSAT

Table 3.4: The X-ray luminosities and catalogs for the objects in Table 3.3.

Name	L_X (cgs)	Catalog
V442 Oph	$2.7 \times 10^{-12} \pm 5.7 \times 10^{-14}$	Webb et al. (2020)
XMMSL2 J185453.6-142834	$1.62 \times 10^{12} \pm 7.86 \times 10^{-13}$	Saxton et al. (2008)
CP Lac	$2.5 \times 10^{-14} \pm 7.9 \times 10^{-15}$	ROSAT (2000)
OR And	$2.0 \times 10^{-13} \pm 7.7 \times 10^{-14}$	Boller et al. (2016)

total there are 40 possible candidates (Table 3.5 above the dashed line). These candidates aren't as strong as those from the ASAS-SN, ZTF, or Rodríguez et al. (2000) datasets because I could not make use of the second type of selection on the PLR.

3.3.1 Candidate selection by amplitude

Another method one could use is selecting all the high-amplitude variables. This is a possible method for Gaia data because of the lack of period in the published tables. This was also a suggestion made by Peterson et al. (2019) to find more AR Sco-like binaries. In Figure 7 of their paper, they plot period vs the amplitude of variable stars. AR Sco is high above the rest, in a small population with amplitude > 1 mag. With this in mind I selected the δ Scutis in Gaia that also had an amplitude > 1 mag. Only three in the entire dataset met this condition and there was no overlap between these and any in Table 3.5. The high-amplitude Gaia variables are shown in Table 3.6. These did not have X-ray or radio counterparts and due to their distance, they cannot be ruled out.

Table 3.5: The list of selected δ Scutis that could not be ruled out from the Gaia sample are above the dashed line. The coordinates are taken from Gaia EDR3 (Gaia Collaboration et al., 2021; Riello et al., 2021) and rounded to the nearest arcsecond.

RA (deg)	Dec (deg)	Distance (pc)
8.6210	73.5583	760 ⁺¹⁰ ₋₁₀
52.7750	20.5862	1630 ⁺¹⁶⁰ ₋₁₃₀
83.7603	-55.8494	2800 ⁺³⁰⁰ ₋₂₀₀
90.4623	69.2913	2300 ⁺³⁰⁰ ₋₃₀₀
95.3357	76.8599	1290 ⁺⁸⁰ ₋₈₀
108.9745	58.2685	1140 ⁺⁶⁰ ₋₅₀
117.7352	-30.1514	1480 ⁺⁵⁰ ₋₆₀
119.7548	-8.1750	1060 ⁺⁴⁰ ₋₃₀
173.2748	-63.5050	2120 ⁺¹⁸⁰ ₋₁₇₀
179.6967	-67.9753	2600 ⁺³⁰⁰ ₋₃₀₀
183.8387	24.7967	960 ⁺⁸⁰ ₋₈₀
187.1244	-22.8827	1680 ⁺¹⁷⁰ ₋₁₇₀
192.4389	4.0272	1410 ⁺⁶⁰ ₋₅₀
222.4613	-44.6693	1350 ⁺⁹⁰ ₋₇₀
227.0699	-38.5410	602 ⁺¹⁴ ₋₁₇
228.3851	-69.8239	1120 ⁺³⁰ ₋₃₀
239.2868	-46.1420	1190 ⁺⁴⁰ ₋₅₀
240.8783	-68.5503	2900 ⁺⁵⁰⁰ ₋₄₀₀
265.6236	20.5129	2300 ⁺⁴⁰⁰ ₋₃₀₀
269.5654	-36.6949	1530 ⁺¹¹⁰ ₋₁₀₀
275.2460	-23.5546	3000 ⁺⁸⁰⁰ ₋₄₀₀
281.3458	12.1102	1260 ⁺⁸⁰ ₋₇₀
282.0054	-49.8814	691 ⁺¹² ₋₈
283.7217	-14.4771	1320 ⁺⁶⁰ ₋₆₀
282.4645	-13.6762	601 ⁺⁸ ₋₈
283.9532	23.0234	2800 ⁺⁵⁰⁰ ₋₃₀₀
293.0205	-11.0341	1540 ⁺¹⁹⁰ ₋₁₉₀
293.2862	9.8322	2300 ⁺³⁰⁰ ₋₂₀₀
294.0792	7.2186	2000 ⁺³⁰⁰ ₋₂₀₀
296.6380	19.6573	1240 ⁺⁴⁰ ₋₄₀
297.8768	22.3498	1410 ⁺⁷⁰ ₋₈₀
316.9423	65.6256	2600 ⁺³⁰⁰ ₋₃₀₀
325.9775	12.7494	1110 ⁺⁶⁰ ₋₅₀
329.5990	52.7586	2300 ⁺³⁰⁰ ₋₃₀₀
336.1806	66.9229	980 ⁺³⁰ ₋₂₀
346.6270	44.3135	616 ⁺¹⁰ ₋₁₁
347.6427	65.0094	720 ⁺¹² ₋₉
48.6108	23.7705	256 ⁺⁸ ₋₁₀
286.6607	-19.1792	240 ⁺² ₋₂
290.0589	27.3717	190.6 ^{+1.1} _{-1.2}

Table 3.6: The three δ Scutis with amplitude > 1 mag. The coordinates are taken from Gaia EDR3 (Gaia Collaboration et al., 2021; Riello et al., 2021) and rounded to the nearest arcsecond.

RA (deg)	Dec (deg)	Distance (pc)
0.05178	24.4358	3800 $^{+500}_{-400}$
238.5308	31.6366	3400 $^{+500}_{-400}$
246.5010	34.8894	4600 $^{+800}_{-500}$

Chapter 4

Population estimate of AR Sco twins in the Milky Way

With the results of the previous chapters, I can attempt to make a population estimate of AR Sco twins in the Galaxy. Admittedly, this will be difficult considering we still currently know of only one. However, I will still estimate this by modeling the distribution of δ Scutis and using this to determine the maximum distance to which each catalog is complete. We will use the most complete to calculate a lower limit and upper limit of high-amplitude δ Scutis (which were the most complete). We find the ratio of δ Scutis to stellar matter and the ratio of known or candidate AR Scos to the number of stars searched. Multiplying these together yields our limits.

4.1 The space density of δ Scutis

The natural choice for a large sample initially was ASAS-SN. I downloaded all the positions for δ Scutis in the ASAS-SN variable star catalog and made histograms of their density in multiple dimensions. The distribution of stars as a function of the distance from the center of the Galaxy is a simple exponential, while the vertical distribution must be modeled by sech^2 . van der Kruit (1988) explain this is from the assumption that the disc of our Galaxy is self-gravitating and isothermal. Since I assumed a distribution as described in van der Kruit (1988), my job was to find the scale height of the distribution. The equation used for the fit is as follows.

$$n(r, z) = n_0 e^{r/R_s} \text{sech}^2(|z|/Z_s). \quad (4.1)$$

For R_s I used a Galactic scale length of 4 kpc (Cox, 2000). I could not immediately assume a scale height because this changes for different populations of stars. To find the most accurate scale height, I first plot the z distribution of δ Scutis with the intention to fit it with a modified version of Equation 4.1. If we integrate n over r , then we are left with

$$n(z) = C \text{sech}^2(|z|/Z_s), \quad (4.2)$$

where C is a constant. I left C and Z_s as free parameters in order to find the best scale height to fit the data. Because dust is an issue at large distances, it is not wise to include all r in the fit to the function above. If we choose a range of limits on r , Z_s first decreases and then around 756 pc, it begins to increase. The increase in scale height is more than likely not real as the scale height should decrease when we add more data points and then hover around its true value. The decrease occurs because at small r , there are still a hand full of stars far above and far below the plane. This flattens the distribution and leads to an erroneously large scale height. Thus, for the scale height, I chose the value it had at $r = 756$ pc, which was 350 ± 20 pc.

The plan was to fit the radial distribution of sources from the Sun and see where the ASAS-SN catalog becomes incomplete. Before doing so, the coordinate origin had to be moved to the Sun rather than the galactic center, so I made a coordinate transformation from cylindrical to cartesian coordinates. Then, I assumed an offset of -8 kpc in x and 13 pc in z . The offset in y was set to 0. Finally I rewrote the equation in Galactic (left-handed spherical) coordinates to continue to the next part of the analysis.

The number of sources in ASAS-SN falls off significantly after roughly 1000 pc so the data beyond that cannot be used for a fit. However, due to the ASAS-SN telescopes saturating at 10 - 11 mag, we know that the catalog must also be incomplete closer than 600 to 1000 pc given the absolute magnitude range of δ Scutis ($M_V \approx 0.8 - 2.7$). Clearly, there is an issue with completeness in

the catalog, which is only more apparent when we compare these sources those in Rodríguez et al. (2000). The distribution of these sources peak well below the peak in the ASAS-SN data (Figures 4.1 and 4.2). We therefore conclude that ASAS-SN is complete nowhere and should not be used to fit the number density function above. ZTF also suffered from this incompleteness issue.

Fitting to the data from Rodríguez et al. (2000) allowed us to determine a reasonable n_0 and then plot the number of δ Scutis at a distance of our choosing. This allows us to determine how incomplete a given catalog is. The fit is shown in Figure 4.1. AR Sco is included in this data as it was classified as a δ Scuti at the time.

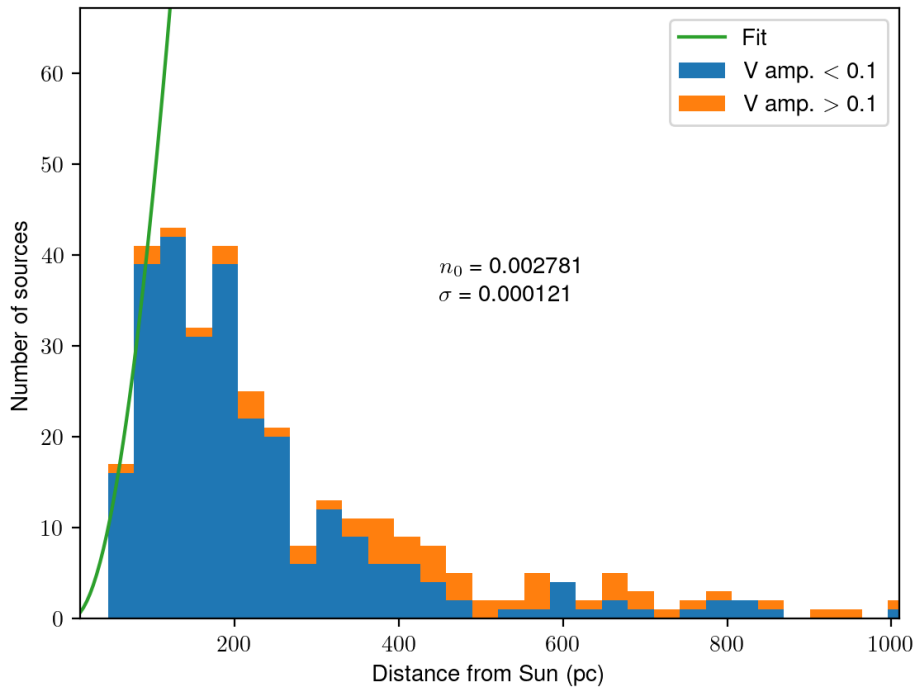


Figure 4.1: The fit for δ Scutis in Rodríguez et al. (2000) AR Sco is indicated by the red star. Each color in the histogram corresponds to a different amplitude. It should be immediately apparent that our high-amplitude stars are not usually found at close distances and are vastly outnumbered.

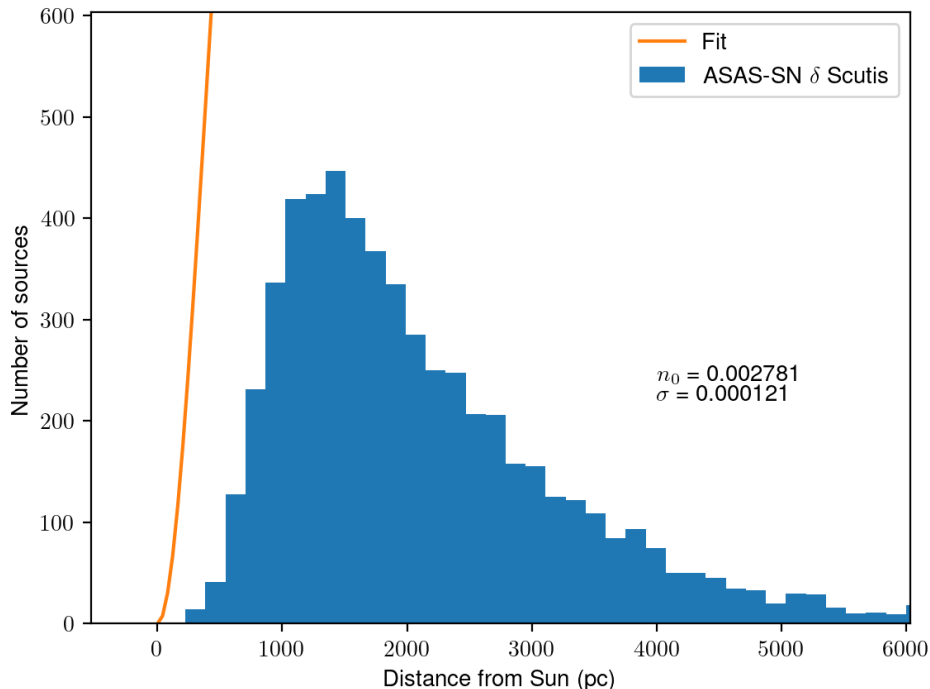


Figure 4.2: The fit of Rodríguez et al. (2000) to the ASAS-SN δ Scutis.

4.2 Completeness of different amplitudes

Before we make any population estimates, let's consider the completeness of each catalog once again. Using the fit to the data from Figure 4.1, we can see that ASAS-SN (Figure 4.2) is very incomplete. However, it is likely that higher amplitude variables are easier to detect at long distances. Since the ASAS-SN catalog of variable stars peaks around 1200 pc, it could be more complete for high-amplitude δ Scutis. To test this, I fit to the Rodríguez et al. (2000) sample again, but only include those with an amplitude above 0.1 mag. This is what I defined as high-amplitude. Using this fit we can compare to the ASAS-SN data for stars of the same amplitude.

The fit calculated in Figure 4.3 applied to Figure 4.4 shows a significant improvement from Figure 4.2. We therefore conclude that ASAS-SN is probably complete for high-amplitude δ Scutis up to ~ 1600 pc. We checked the completeness of ZTF for high-amplitude δ Scutis and found that the model

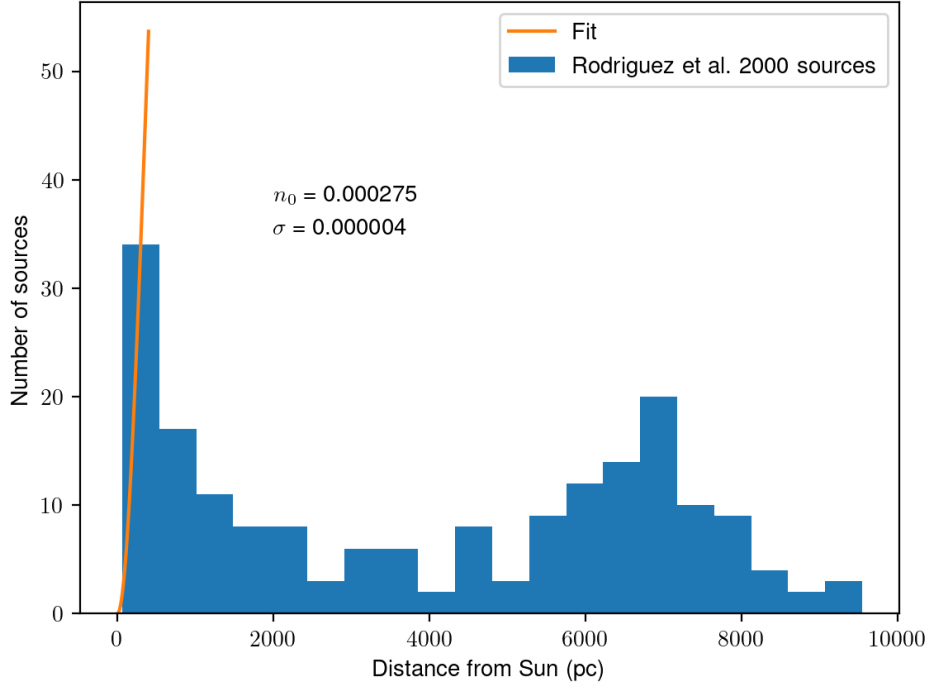


Figure 4.3: The fit to only the high-amplitude δ Scutis from Rodríguez et al. (2000).

was decently similar to the data (see Figure 4.5). It seems that at close distances (below 2 kpc), ZTF suffers from saturation, however. Rather than using the full dataset for the population lower and upper limits then, we can use the high-amplitude portion as finding one high-amplitude δ Scuti probes more space than a single δ Scuti.

A note on the fit in Figure 4.3: changing the bin size did not drastically change n_0 . While there are not many data points to use for a fit when I limited the amplitude in the Rodríguez et al. (2000) sample, it is encouraging that when the number of bins is increased (and some of the slow increase is revealed near the Sun), that the fit is nearly the same.

4.3 Population lower limit

Since the high-amplitude portion of Rodríguez et al. (2000) includes AR Sco, I used this to estimate a lower limit on the number of AR Sco twins in the

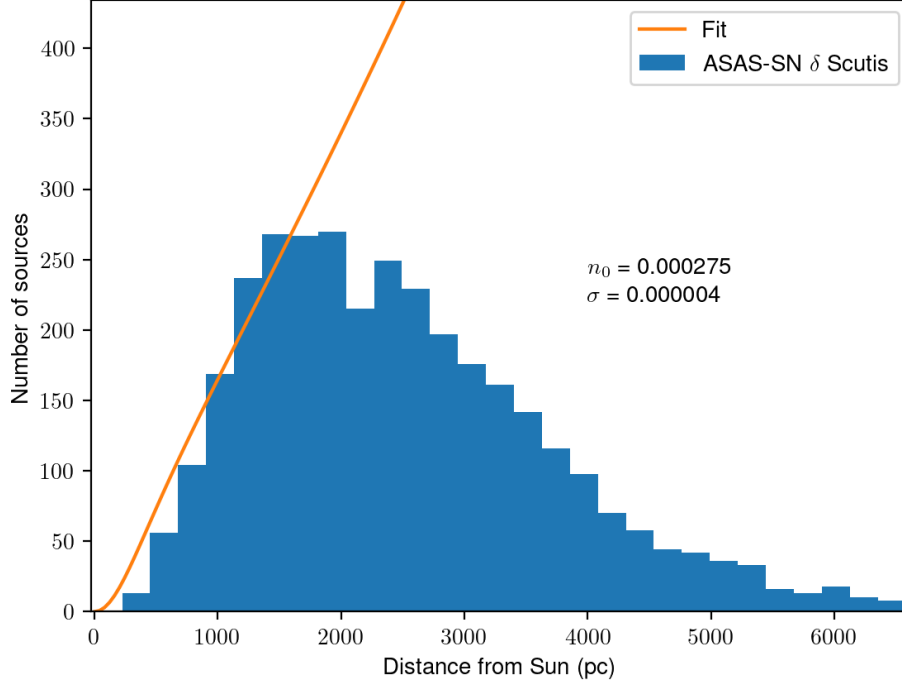


Figure 4.4: The fit from Figure 4.3 to high-amplitude ASAS-SN δ Scutis.

Galaxy. I used the portion of the Rodríguez et al. (2000) catalog I determined to be complete (298.73 pc) to find a ratio of the number of δ Scutis to stellar mass in the Galaxy at that distance. The initial density of stellar matter near the Sun as reported in McKee et al. (2015) is $0.043M_{\odot}\text{pc}^{-3}$ so,

$$M_{298pc} = \frac{4}{3}\pi(298.73 \text{ pc})^3 \cdot 0.043M_{\odot} \text{ pc}^{-3} = 4.80 \times 10^6 M_{\odot}.$$

We've assumed that the scale height of the number of stars in the Galaxy would not matter at such short distances, so I used the equation for the volume of a sphere. Summing the total number of high-amplitude δ Scutis from Rodríguez et al. (2000) and ASAS-SN within 298.73 pc (there were none in ZTF), we know that there are 37 for every $4.80 \times 10^6 M_{\odot}$ in the Galaxy. We also know that there was one confirmed AR Sco within this catalog so we have 1 AR Sco per 83 high-amplitude δ Scutis in Rodríguez et al. (2000) alone. In order to estimate the 2σ lower limit, we use the 2σ lower limit on 1 detection, which is 0.023 (Gehrels, 1986). This is our first ratio, which the reader should

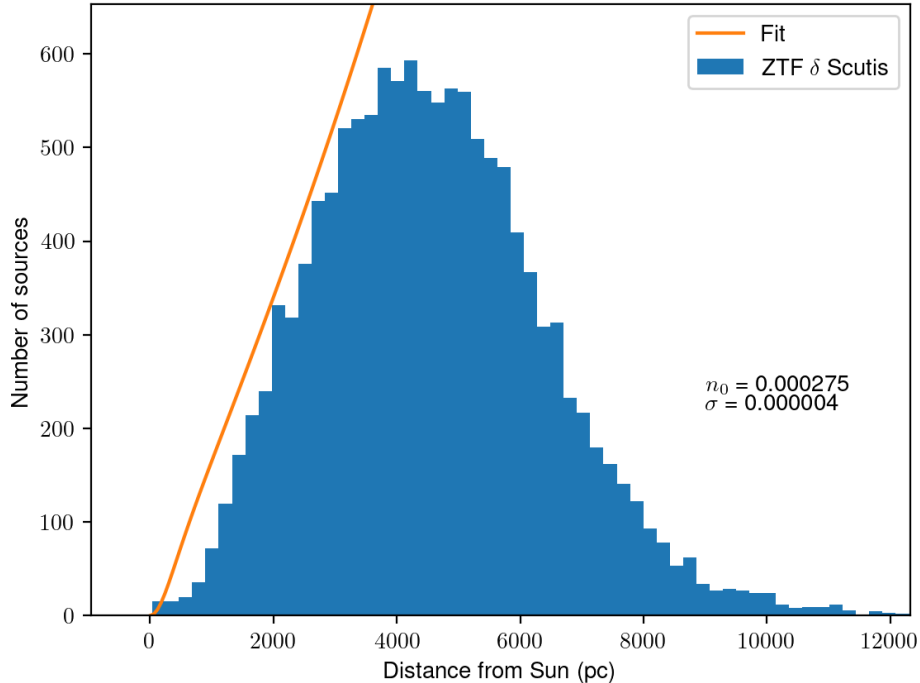


Figure 4.5: The fit from Figure 4.3 to high-amplitude ZTF δ Scutis.

know only includes the number of high-amplitude δ Scutis searched. Since our method included crossmatching with 2MASS and Gaia, the number of sources thrown out was significant. As such we will limit ourselves to the population that truly was searched. Multiplying our two ratios together we get 2.1×10^{-9} AR Scos M_{\odot}^{-1} . Licquia & Newman (2015) report the total stellar mass in our Galaxy is $6.08 \times 10^{10} M_{\odot}$. Thus, the lower limit on the number of AR Scos in our Galaxy is 130.

4.4 Population upper limit using ASAS-SN, ZTF, and Rodríguez et al. (2000)

The candidates in Table 2.2 and 3.2 are definitely not all AR Sco twins. In fact, it is likely none of them are. However, if we imagine that each one of them is, then we can use them to find an upper limit on the number of AR Scos in the Galaxy that could be mistaken for δ Scutis. Just as with the

lower limit, we will only consider those with an amplitude above 0.1 mag. Since there are only stars classified by ASAS-SN as high-amplitude δ Scutis and uncertain δ Scutis in Table 2.2, we can only use these parts of ASAS-SN for this estimate. There are 3444 of these sources combined and 5 possible high-amplitude candidates from the table. As for ZTF, there are 12 possible candidates out of 5749. We now combine this with the one known AR Sco plus the 1 possible candidate and 342 δ Scutis from Rodríguez et al. (2000). The 2σ upper limit on 17 detections (the total number of high-amplitude possible candidates) is ~ 27.44 (Gehrels, 1986). Thus,

$$\frac{27.44 \text{ AR Scos}}{9535 \delta \text{ Scutis}} \cdot \frac{37 \delta \text{ Scutis}}{4.80 \times 10^6 M_{\odot}} = 2.22 \times 10^{-8} \text{ AR Scos } M_{\odot}^{-1} \quad (4.3)$$

and multiplying by the mass of the Galaxy once again we have an upper limit of 1.3×10^3 AR Sco twins. It would be fine to add in the AR Sco candidate twin ZTF18abnbzvx (Kato & Kojiguchi, 2021), but it would not change the result by a significant amount.

4.5 Comparison to quiescent BHXB population

As mentioned in the introduction, Tetarenko et al. (2016) argued that VLA J2130+12 is the first low-mass BHXB found outside of a globular cluster in a quiescent state. The authors estimate that there are between 2.6×10^4 - 1.7×10^8 radio sources like VLA J2130+12 in the Galaxy at the 3σ level (considering small number statistics). That translates to 4.5×10^5 - 7.4×10^7 at the 2σ level. They explain that their lower limit corresponds to the estimates of quiescent BHXBs from population synthesis models and conclude that the models are underestimating the number of systems like what they discovered. We considered that some of these bright radio sources in the Galaxy could be explained at least in part by AR Sco twins. However, if I compare the 2σ estimates for both, there is no overlap. The 2σ lower limit for radio sources like VLA J2130+12 is two orders of magnitude higher than the 2σ upper limit on AR Sco twins (1.3×10^3).

Chapter 5

Conclusion

While I have not found any likely candidates for an AR Sco twin, this thesis provides a few deliverables, the most important being the method I designed to find AR Sco twins, which was outlined in Chapter 2. Using this method, I found 21 possible candidates from ASAS-SN, ZTF, and Rodríguez et al. (2000) that could not be ruled out based on non-detections in archival X-ray and radio data. The method I presented in Chapter 2 that discovered these should be trusted as part of a search for AR Sco twins. The regions on the PLR and CMD in which I found the possible candidates are uncharacteristic for δ Scutis and I have shown that they have CV contamination to different degrees. One that showed up in ASAS-SN was QS Vir, and I will discuss this more later. This is encouraging as I was indeed hoping to find WD/red dwarf binaries in our datasets. In addition, I was able to recover AR Sco itself as a proof-of-concept when examining data in Rodríguez et al. (2000).

One of the possible candidates from ZTF turned out to be very interesting, although there was no radio counterpart. 2SXPS 169712 showed two peaks in the X-ray (Figure 3.8), which are about 120 days apart. Coupled with the luminosity change between the rough position of the lowest and highest points, this most closely resembles a dwarf nova outbursts.

We also examined Gaia DR2 data as part of our search, but unfortunately the data do not result in a reliable Fourier decomposition. Without this, I could not perform our selection on the PLR. As a result I was left with a rather large and untrustworthy amount of possible candidates. While the selection I made

on the CMD (Figure 3.9) did include some known CVs, the rest were mostly impossible to rule out. Knowing the period of each of these is an important part of the method, which should probably be included in future analysis. I also selected stars in Gaia DR2 that had amplitudes above 1 magnitude. This resulted in 3 possible, but unlikely candidates since they did not have X-ray or radio counterparts and did not correspond to any of the sources from the CMD selection.

Given how many candidates I have, I calculated an estimate on the number of AR Sco-like systems there could be in the Galaxy. As each seemed to be more complete for δ Scutis with an amplitude greater than 0.1 mag, I surmised that a discovery of one high-amplitude star probed a larger region of space. Hence with the lower and upper limits, I only used these. The lower limit I found was 130 and the upper limit was 1.3×10^3 . This is an extraordinarily small number compared to the number of possible radio-bright sources in the Galaxy. AR Sco twins are likely only able to explain a small part of this population.

It is unlikely that most of the possible candidates are AR Sco twins, but in order to say that with certainty, one would need to conduct some follow-up observations to rule any of them out. To determine whether any of these have X-ray counterparts, a good option is the Chandra X-ray Observatory. Its sensitivity and spatial resolution would provide a confident detection or non-detection. For radio, I would suggest the VLA as filler targets. Hour-long observations can be worked in easily. The key way to rule out any of our possible candidates would be high-cadence observations at optical wavelengths in order to detect a signal from a spinning WD. Using Gemini for this purpose is part of our plan for the future.

We can now turn to the radio counterpart of QS Vir mentioned above. We discovered QS Vir among the uncertain δ Scutis in ASAS-SN. As part of our method I queried the VLASS-QL catalog and found that there was a point source less than an arcsecond away from its coordinates in Gaia EDR3. The flux was found to be $980 \pm 160 \mu$ Jy. At this time I know of no reported radio counterpart for QS Vir. Since the radio study of CVs is a relatively new field,

I will conduct an archival radio search of CVs in the future. The main hurdle would be to narrow down the ridiculous number of known CVs from facilities like ZTF. One way to handle this is to limit the search to 100 pc or so as a start.

References

- Astropy Collaboration, Price-Whelan, A. M., Sipőcz, B. M., et al. 2018, *AJ*, 156, 123, doi: 10.3847/1538-3881/aabc4f
- Bahramian, A., Miller-Jones, J., Strader, J., et al. 2018, Radio/X-ray correlation database for X-ray binaries, v0.1, Zenodo, doi: 10.5281/zenodo.1252036. <https://doi.org/10.5281/zenodo.1252036>
- Bailer-Jones, C. A. L., Rybizki, J., Fouesneau, M., Demleitner, M., & Andrae, R. 2021, *AJ*, 161, 147, doi: 10.3847/1538-3881/abd806
- Bailer-Jones, C. A. L., Rybizki, J., Fouesneau, M., Mantelet, G., & Andrae, R. 2018, *AJ*, 156, 58, doi: 10.3847/1538-3881/aacb21
- Bellm, E. C., Kulkarni, S. R., Graham, M. J., et al. 2019, *PASP*, 131, 018002, doi: 10.1088/1538-3873/aaecbe
- Boller, T., Freyberg, M. J., Trümper, J., et al. 2016, *A&A*, 588, A103, doi: 10.1051/0004-6361/201525648
- Bookbinder, J. A., & Lamb, D. Q. 1987, *ApJL*, 323, L131, doi: 10.1086/185072
- Bowman, D. M. 2017, *Amplitude Modulation of Pulsation Modes in Delta Scuti Stars* (Cham, Switzerland: Springer International Publishing), doi: 10.1007/978-3-319-66649-5
- Bradt, H. 2008, *Astrophysics Processes* (New York: Cambridge University Press)
- Buckley, D. A. H., Meintjes, P. J., Potter, S. B., Marsh, T. R., & Gänsicke, B. T. 2017, *Nature Astronomy*, 1, 0029, doi: 10.1038/s41550-016-0029
- Burrows, D. N., Hill, J. E., Nousek, J. A., et al. 2000, in *Society of Photo-Optical Instrumentation Engineers (SPIE) Conference Series*, Vol. 4140, X-Ray and Gamma-Ray Instrumentation for Astronomy XI, ed. K. A. Flanagan & O. H. Siegmund, 64–75
- Burrows, D. N., Hill, J. E., Nousek, J. A., et al. 2005, *Space Sci. Rev.*, 120, 165, doi: 10.1007/s11214-005-5097-2
- Carroll, B. W., & Ostlie, D. A. 2007, *An Introduction to Modern Astrophysics* (San Francisco: Pearson)
- Cox, A. N. 2000, *Allen’s astrophysical quantities* (New York: AIP Press, Springer)

- Dimitrijević, M. S., Kovačević, A., Simić, Z., & Sahal-Bréchet, S. 2011, *Baltic Astronomy*, 20, 495, doi: 10.1515/astro-2017-0327
- Dubus, G., Otulakowska-Hypka, M., & Lasota, J.-P. 2018, *A&A*, 617, A26, doi: 10.1051/0004-6361/201833372
- Evans, P. A., Beardmore, A. P., Page, K. L., et al. 2007, *A&A*, 469, 379, doi: 10.1051/0004-6361:20077530
- . 2009, *MNRAS*, 397, 1177, doi: 10.1111/j.1365-2966.2009.14913.x
- Eyer, L., Mowlavi, N., Evans, D. W., et al. 2017, arXiv e-prints, arXiv:1702.03295. <https://arxiv.org/abs/1702.03295>
- Ferrario, L., de Martino, D., & Gänsicke, B. T. 2015, *Space Sci. Rev.*, 191, 111, doi: 10.1007/s11214-015-0152-0
- Gaia Collaboration, Prusti, T., de Bruijne, J. H. J., et al. 2016, *A&A*, 595, A1, doi: 10.1051/0004-6361/201629272
- Gaia Collaboration, Brown, A. G. A., Vallenari, A., et al. 2018, *A&A*, 616, A1, doi: 10.1051/0004-6361/201833051
- Gaia Collaboration, Eyer, L., Rimoldini, L., et al. 2019, *A&A*, 623, A110, doi: 10.1051/0004-6361/201833304
- Gaia Collaboration, Brown, A. G. A., Vallenari, A., et al. 2021, *A&A*, 649, A1, doi: 10.1051/0004-6361/202039657
- Garnavich, P., Littlefield, C., Kafka, S., et al. 2019, *ApJ*, 872, 67, doi: 10.3847/1538-4357/aafb2c
- Gehrels, N. 1986, *ApJ*, 303, 336, doi: 10.1086/164079
- Geier, S., Raddi, R., Gentile Fusillo, N. P., & Marsh, T. R. 2019, *A&A*, 621, A38, doi: 10.1051/0004-6361/201834236
- Geng, J.-J., Zhang, B., & Huang, Y.-F. 2016, *ApJ*, 831, L10, doi: 10.3847/2041-8205/831/1/L10
- Goad, M. R., Tyler, L. G., Beardmore, A. P., et al. 2007, *A&A*, 476, 1401, doi: 10.1051/0004-6361:20078436
- Hansen, C. J., Kawaler, S. D., & Trimble, V. 2004, *Stellar interiors : physical principles, structure, and evolution* (New York: Springer-Verlag)
- Hellier, C. 2001, *Cataclysmic Variable Stars: How and Why They Vary* (Berlin: Springer)
- Jayasinghe, T., Kochanek, C. S., Stanek, K. Z., et al. 2018, *MNRAS*, 477, 3145, doi: 10.1093/mnras/sty838
- Jayasinghe, T., Stanek, K. Z., Kochanek, C. S., et al. 2019, *MNRAS*, 486, 1907, doi: 10.1093/mnras/stz844
- Jayasinghe, T., Stanek, K. Z., Kochanek, C. S., et al. 2019a, *MNRAS*, 485, 961, doi: 10.1093/mnras/stz444

- Jayasinghe, T., Stanek, K. Z., Kochanek, C. S., et al. 2020, MNRAS, 493, 4186, doi: 10.1093/mnras/staa499
- Kato, T., & Kojiguchi, N. 2021, arXiv e-prints, arXiv:2107.09913. <https://arxiv.org/abs/2107.09913>
- Katz, J. I. 2017, ApJ, 835, 150, doi: 10.3847/1538-4357/835/2/150
- Kochanek, C. S., Shappee, B. J., Stanek, K. Z., et al. 2017, PASP, 129, 104502, doi: 10.1088/1538-3873/aa80d9
- Lacy, M., Baum, S. A., Chandler, C. J., et al. 2020, PASP, 132, 035001, doi: 10.1088/1538-3873/ab63eb
- Lasota, J.-P. 2001, New Astronomy Reviews, 45, 449, doi: 10.1016/S1387-6473(01)00112-9
- Licquia, T. C., & Newman, J. A. 2015, ApJ, 806, 96, doi: 10.1088/0004-637X/806/1/96
- Lyutikov, M., Barkov, M., Route, M., et al. 2020, arXiv e-prints, arXiv:2004.11474. <https://arxiv.org/abs/2004.11474>
- Madore, B. F. 1982, ApJ, 253, 575, doi: 10.1086/159659
- Mahabal, A., Rebbapragada, U., Walters, R., et al. 2019, PASP, 131, 038002, doi: 10.1088/1538-3873/aaf3fa
- Marsh, T. R., Gänsicke, B. T., Hümmerich, S., et al. 2016, Nature, 537, 374, doi: 10.1038/nature18620
- McKee, C. F., Parravano, A., & Hollenbach, D. J. 2015, ApJ, 814, 13, doi: 10.1088/0004-637X/814/1/13
- Mittaz, J. P. D., Rosen, S. R., Mason, K. O., & Howell, S. B. 1992, MNRAS, 258, 277, doi: 10.1093/mnras/258.2.277
- Osaki, Y. 1974, PASJ, 26, 429
- Patterson, J., Masi, G., Richmond, M. W., et al. 2002, PASP, 114, 721, doi: 10.1086/341696
- Peterson, E., Littlefield, C., & Garnavich, P. 2019, AJ, 158, 131, doi: 10.3847/1538-3881/ab2ad5
- Pretorius, M. L., Hewitt, D. M., Woudt, P. A., et al. 2021, MNRAS, 503, 3692, doi: 10.1093/mnras/stab498
- Ramsay, G., Cropper, M., Mason, K. O., Córdova, F. A., & Priedhorsky, W. 2004, MNRAS, 347, 95, doi: 10.1111/j.1365-2966.2004.07242.x
- Richards, J. W., Starr, D. L., Butler, N. R., et al. 2011, ApJ, 733, 10, doi: 10.1088/0004-637X/733/1/10
- Riello, M., De Angeli, F., Evans, D. W., et al. 2021, A&A, 649, A3, doi: 10.1051/0004-6361/202039587
- Rimoldini, L., Holl, B., Audard, M., et al. 2019, A&A, 625, A97, doi: 10.1051/0004-6361/201834616

- Robinson, E. L. 1976, *ARA&A*, 14, 119, doi: 10.1146/annurev.aa.14.090176.001003
- Rodríguez, E., López-González, M. J., & López de Coca, P. 2000, *Astronomy & Astrophysics, Supplement*, 144, 469, doi: 10.1051/aas:2000221
- ROSAT, C. 2000, *VizieR Online Data Catalog*, IX/30
- Satyvaldiev, V. 1971, *Astronomicheskij Tsirkulyar*, 633, 7
- Saxton, R. D., Read, A. M., Esquej, P., et al. 2008, *A&A*, 480, 611, doi: 10.1051/0004-6361:20079193
- Schreiber, M. R., Belloni, D., Gänsicke, B. T., Parsons, S. G., & Zorotovic, M. 2021, *Nature Astronomy*, 5, 648, doi: 10.1038/s41550-021-01346-8
- Shappee, B. J., Prieto, J. L., Grupe, D., et al. 2014, *ApJ*, 788, 48, doi: 10.1088/0004-637X/788/1/48
- Singh, K. K., Meintjes, P. J., & Yadav, K. K. 2021, arXiv e-prints, arXiv:2103.11602. <https://arxiv.org/abs/2103.11602>
- Takata, J., Hu, C. P., Lin, L. C. C., et al. 2018, *ApJ*, 853, 106, doi: 10.3847/1538-4357/aaa23d
- Taylor, M. B. 2005, in *Astronomical Society of the Pacific Conference Series*, Vol. 347, *Astronomical Data Analysis Software and Systems XIV*, ed. P. Shopbell, M. Britton, & R. Ebert, 29
- Tetarenko, B. E., Bahramian, A., Arnason, R. M., et al. 2016, *ApJ*, 825, 10, doi: 10.3847/0004-637X/825/1/10
- van der Kruit, P. C. 1988, *A&A*, 192, 117
- Voges, W., Aschenbach, B., Boller, T., et al. 1999, *A&A*, 349, 389. <https://arxiv.org/abs/astro-ph/9909315>
- Wargau, W. F. 1985, *The Messenger*, 40, 7
- Warner, B. 2003, *Cataclysmic Variable Stars* (Cambridge, UK: Cambridge University Press), doi: 10.1017/CB09780511586491
- Watson, C. L., Henden, A. A., & Price, A. 2006, *Society for Astronomical Sciences Annual Symposium*, 25, 47
- Webb, N. A., Coriat, M., Traulsen, I., et al. 2020, *A&A*, 641, A136, doi: 10.1051/0004-6361/201937353
- Wickramasinghe, D. T., & Ferrario, L. 2005, *MNRAS*, 356, 1576, doi: 10.1111/j.1365-2966.2004.08603.x
- Wynn, G. A., King, A. R., & Horne, K. 1997, *MNRAS*, 286, 436, doi: 10.1093/mnras/286.2.436
- Zorotovic, M., & Schreiber, M. R. 2020, *Advances in Space Research*, 66, 1080, doi: 10.1016/j.asr.2019.08.044